Observed Microphysical Evolution for Two East Coast Winter Storms and the Associated Snow Bands

DAVID STARK AND BRIAN A. COLLE

School of Marine and Atmospheric Sciences, Stony Brook University, Stony Brook, New York

SANDRA E. YUTER

Department of Marine, Earth, and Atmospheric Sciences, North Carolina State University, Raleigh, North Carolina

(Manuscript received 21 September 2012, in final form 18 December 2012)

ABSTRACT

This paper presents the observed microphysical evolution of two coastal extratropical cyclones (19–20 December 2009 and 12 January 2011) and the associated passage of heavy snowbands in the cyclone comma head. The observations were made approximately 93 km east of New York City at Stony Brook, New York. Surface microphysical measurements of snow habit and degree of riming were taken every 15–30 min using a stereo microscope and camera, and snow depth and snow density were also recorded. A vertically pointing Ku-band radar observed the vertical evolution of reflectivity and Doppler vertical velocities. There were rapid variations in the snow habits and densities related to the changes in vertical motion and depth of saturation. At any one time, a mixture of different ice habits was observed. Certain ice habits were dominant at the surface when the maximum vertical motion aloft occurred at their favored temperature for depositional growth. Convective seeder cells above 4 km MSL resulted in relatively cold (less than −15°C) ice crystal habits (side planes, bullets, and dendrites). Needlelike crystals were prevalent during the preband period when the maximum vertical motion was in the layer from −5° to −10°C. Moderately rimed dendritic crystals were observed at snowband maturity associated with the strongest frontogenetical ascent on the warm (east) side of the bands. Riming rapidly decreased and more platelike crystals became more numerous as the strongest ascent moved east of Stony Brook. Snow-to-liquid density ratios ranged from 8:1 to 13:1 in both events, except during the period of graupel, when the ratio was as low as 4:1.

1. Introduction

a. Background

Coastal extratropical cyclones (e.g., nor'easters) impact millions of people along the east coast of the United States during the cool season. Heavy snow and mixed precipitation from these winter storms can shut down basic transportation and public services. For example, on 12–14 March 1993, an intense coastal storm affected the entire eastern seaboard (Kocin et al. 1995), with some locations receiving over 100 cm of snowfall. Travel was significantly disrupted, and damage was estimated to exceed $2 billion (Kocin et al. 1995). On 11–12 February 2006, the New York City (NYC) metropolitan area received 8–10 cm h^{-1} snowfall rates, which created dangerous driving conditions from blowing snow and near zero visibilities [(National Climatic Data Center) NCDC 2006].

Much of the small-scale variations in heavy snowfall within extratropical cyclones occurs within snowbands (Novak et al. 2004), which are challenging to forecast in terms of their location and intensity (Novak and Colle 2012). Novak et al. (2004) showed that 85% of extratropical cyclones over the northeast United States during the cool season (October–April) exhibited some type of mesoscale precipitation banding. Of these banding events, 64% had single bands in the northwest quadrant of the extratropical cyclone. Novak et al. (2008) found that band formation occurs in conjunction with a sharpening midlevel trough and associated frontogenesis and a decrease in moist symmetric stability. Novak et al. (2008) also illustrated how the advection of snow can displace the horizontal location of a given snowfall intensity

Corresponding author address: Dr. Brian A. Colle, School of Marine and Atmospheric Sciences, Stony Brook University, Stony Brook, NY 11794-5000.
E-mail: brian.colle@stonybrook.edu

DOI: 10.1175/MWR-D-12-00276.1

between 3 km above mean sea level (MSL) and the surface by ~25 km.

Snowfall accumulation is highly dependent on the snow density, which is in part determined by the ice crystal habit and riming (Roebber et al. 2003). Magono and Lee (1966, see their Fig. 2), Hobbs (1975, see his Table 2), Stoelinga et al. (2007, see their Fig. 5), and Bailey and Hallett (2009, see their Fig. 5) showed that both the temperature and the amount of supersaturation determine ice habit. Other factors that impact snow density include growth rates and size of ice crystals (Ryan et al. 1976; Takahashi et al. 1991), subcloud processes occurring as the crystals fall such as sublimation and melting (Roebber et al. 2003), and compaction at ground level (Roebber et al. 2003). A snow density of 100 kg m^{-3} (10:1) is commonly used by forecasters (Roebber et al. 2003); however, measurements have shown that snow density can vary from as low as ~10 kg m^{-3} (100:1 snow-to-liquid ratio) to as high as ~290 kg m^{-3} (2.9:1) (Power et al. 1964; Super and Holroyd 1997; Judson and Doesken 2000; Roebber et al. 2003). A 30-yr climatology (1971–2000) of snow density across the contiguous United States found a mean snow-to-liquid ratio of 13:1 with considerable variation in the mean (Baxter et al. 2005). The mean 30-yr snow-to-liquid ratio around the New York and Long Island metropolitan area was 10.6:1 with a standard deviation of 5.9:1 (Baxter et al. 2005).

There have been many field campaigns during the past few decades in which in situ cloud microphysics data have been collected. Many of these field studies of cloud microphysics at midlatitudes have occurred over mountainous terrain and within mixed phase clouds including the Cascade Project (Hobbs 1975), the Cyclonic Extratropical Storms (CYCLES) project (Houze et al. 1979), and the Improvement of Microphysical Parameterization through Observational Verification Experiment (IMPROVE; Stoelinga et al. 2003). Along the east coast of the United States and eastern Canada, the ice habit, riming, and size of precipitation particles were examined in three primary field studies. Sienkiewicz et al. (1989) used aircraft data and found mostly dendrites within a frontal snowband. The ground observations obtained during the Canadian Atlantic Storms Program II (CASP II; Stewart and Crawford 1995) exhibited riming ranging from light to heavy and there was often a mixture of ice habits, including varying proportions of ice pellets, plates, and dendrites. The Canadian *CloudSat/Cloud–Aerosol Lidar and Infrared Pathfinder Satellite Observations (CALIPSO)* Validation Project (C3VP; Petersen et al. 2007; Molthan et al. 2010) use both ground and aircraft observations. The C3VP snowstorms contained mostly dendritic crystals with generally light riming.

b. *Motivation*

Previous studies of the microphysics within winter storms over the eastern United States and Canada have revealed large variations in the observed microphysics. There are no published studies along the east coast of the United States documenting the ice habit, riming, and snow density at the surface during the full evolution of a winter storm. Given the rapid changes in vertical motion aloft, we hypothesize that there are associated rapid changes in the surface ice habits, riming, and snow density as a snowband crosses a location. Relatively large errors and uncertainties have been documented within bulk microphysical parameterizations (BMPs) in mesoscale models (Colle et al. 2005; Garvert et al. 2005; Lin and Colle 2009). To improve precipitation forecasts and BMPs for winter storms in general and snowbands in particular, more in situ observations of ice microphysics are needed. By examining the microphysical evolution of snowfall at the surface for two nor'easter events, this paper will address the following questions:

- What is the microphysical evolution along the coast for two nor'easter events?
- How are some of the rapid transitions in ice crystal habit, riming, snow density, and fall speed during these events related to changes in the temperature, moisture, and vertical motion profiles?
- How does the microphysics vary across a snowband within the comma head of the cyclone?

The next section of this paper will discuss the data and methods. Section 3 will focus on the 19–20 December 2009 event from the synoptic scale to the observed microphysics, Section 4 will focus on the 12 January 2011 event, and section 5 will present the conclusions.

2. Data and methods

a. *Instrumentation and datasets*

Detailed microphysical and radar observations for this study were taken at Stony Brook, New York (SBNY), which is on the north shore of Long Island, approximately 93 km east of NYC (Fig. 1). A vertically pointing METEK Ku-band micro rain radar (1.25 cm, MRR; Peters et al. 2002) was used at SBNY to observe the vertical profile of reflectivity and Doppler velocities at 250-m gates spacing in the vertical to 7.5 km MSL every minute. We postprocessed the raw Doppler spectra data files using the method of Maahn and Kollias (2012). This postprocessing corrects for noise and aliasing effects and improves the data quality of the radar reflectivity and Doppler velocity measurements. Additionally, the Maahn and Kollias (2012) postprocessing calculates Doppler

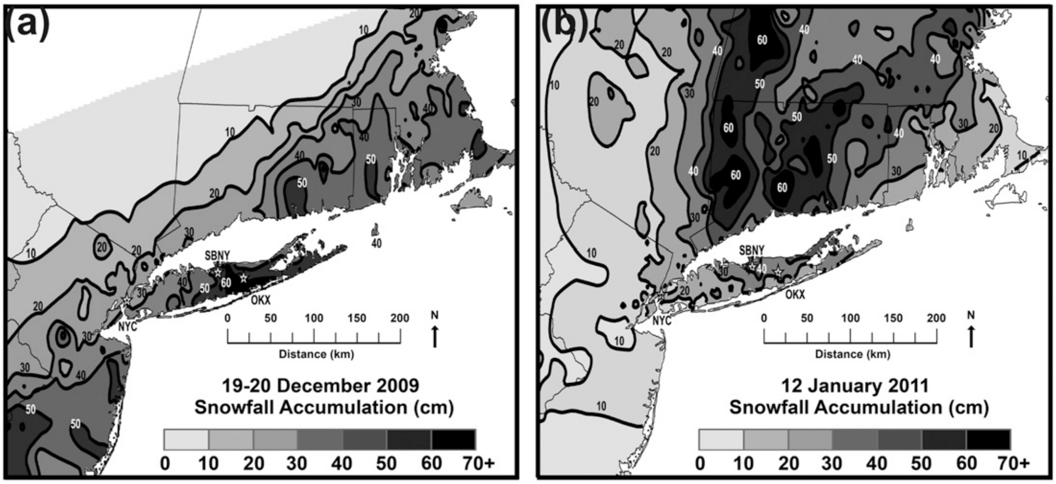

FIG. 1. Storm total snowfall accumulations (shaded and contoured every 10 cm) for the (a) 19–20 Dec 2009 and (b) 12 Jan 2011 snow events. The locations for New York City (NYC), Stony Brook, NY (SBNY), and the NWS forecast office at Upton, NY (OKX), are indicated by the stars.

spectral width σ, a measure of the standard deviation of the distribution of Doppler velocities. The MRR has been used to study snow and winter storms in locations around the world (Peters et al. 2002, 2005; Yuter et al. 2008; Cha et al. 2009; Keighton et al. 2009; Kneifel et al. 2011a,b; Xie et al. 2012; Maahn and Kollias 2012). Attenuation effects can be generally neglected for snow observations at K band (Matrosov 2007). However, in circumstances of heavy snowfall, snow can accumulate on the MRR's heated antenna yielding substantial attenuation (Maahn and Kollias 2012). Periods subject to this type of attenuation are noted in the upcoming data analysis. Doppler velocity from the MRR represents the sum of particle fall speed and vertical air motion. For vertically pointing radars, the two primary sources of σ are turbulence and differential fall velocities (Rinehart 2004). In snow, the larger contributor is usually turbulence, which is associated with both updrafts and boundary layer eddies.

To observe the snow habit and riming intensity at the MRR site, snow crystals were collected using a stereo microscope and camera as described in the next section. The snow depth and snow density were measured several times during the storm. Snow density was obtained by melting snow that had fallen into a circular pan and measuring the change in snow to water volume. Collection issues that could have affected snow density measurements include compaction and melting inside the pan. The evolving precipitation structures were examined using vertical and horizontal cross sections produced using data from the National Weather Service (NWS) Weather Surveillance Radar-1988 Doppler (WSR-88D) radar at Upton, New York (OKX in Fig. 1), which is ~25 km from the MRR site. A complete volume scan from KOKX is produced every 4–6 min. Radiosonde observations from OKX launched every 6–12 h provided vertical profiles of thermodynamic characteristics. The OKX observations were used to verify vertical profiles of temperature and moisture from gridded model analysis over the region. Gridded analyses every 1–6 h and short-term forecasts (3–12 h) from the 13-km Rapid Update Cyclone (RUC; Benjamin et al. 2004) for the 2100 UTC 19 December 2009 forecast cycle and the 12-km North American Mesoscale Model (NAM) 0600 UTC 12 January 2011 forecast cycle provided information on the synoptic and mesoscale wind, temperature, pressure, and moisture across the region. These particular time periods and models had the best representation of the thermal and moisture profiles, precipitation field, and snowband positions for the two respective events.

b. *Snow habit observation methodology*

The methodology for observing snow habit follows that of Stoelinga et al. (2007). During the 2009/10, 2010/11, and 2011/12 cool seasons (from December to March), we observed snow crystals under a stereo microscope for a total of 15 storm events. The two events for this paper were selected, since they had the most pronounced snowbands that crossed SBNY. Crystals were collected on a cold glass plate every 15–30 min and immediately examined under the stereo microscope in an unheated outdoor shed. The temperatures and relative humidity inside the shed were similar to the outdoor readings. We obtained a few samples during the 15–30-min time period in order to get a representative distribution of ice habits and riming. Typical samples contained 25 or more individual crystals. Once under the microscope, the

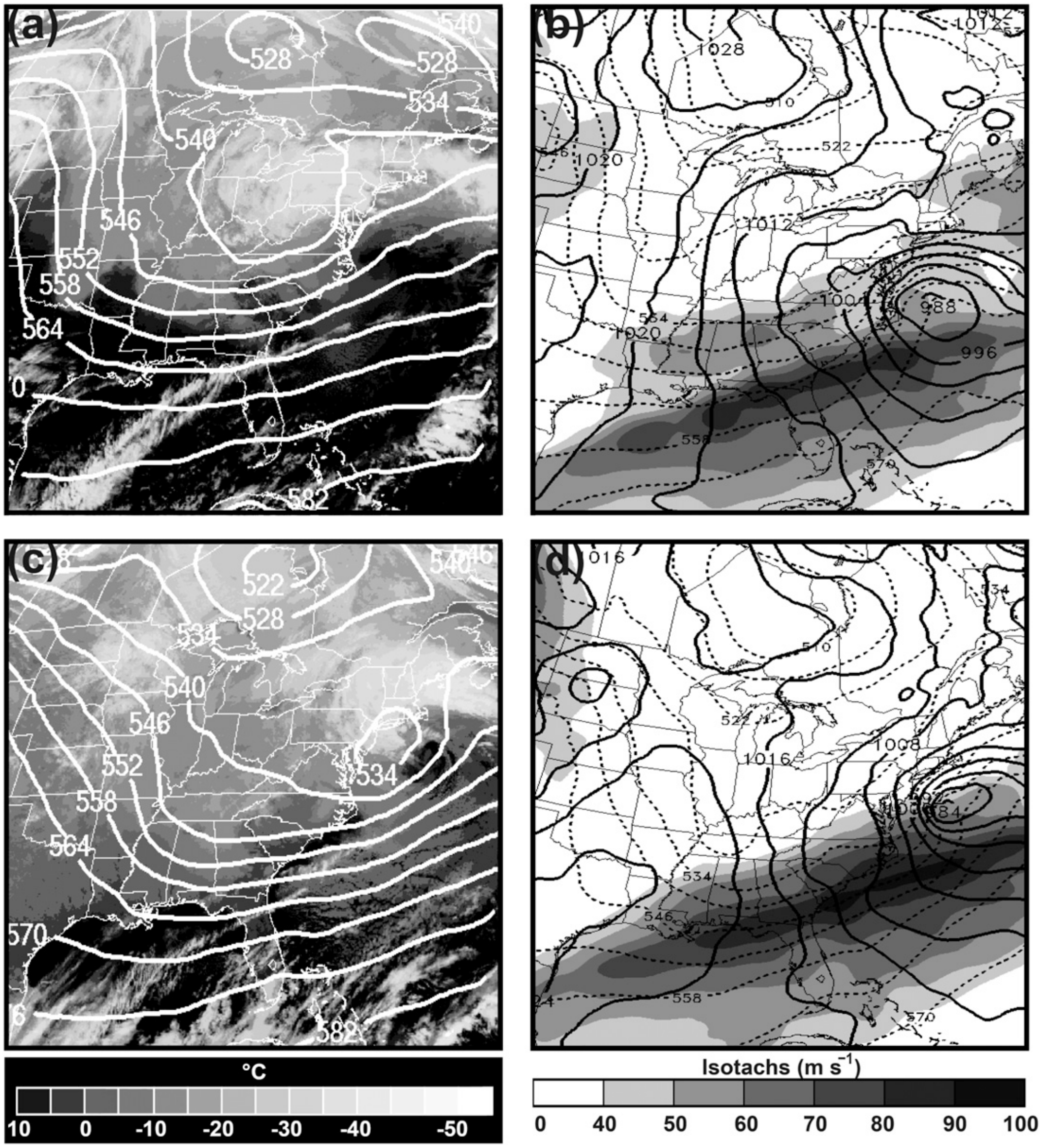

FIG. 2. (a) *Geostationary Operational Environmental Satellite-12* (*GOES-12*) infrared satellite brightness temperature (°C, shaded) and 13-km RUC analysis of 500-hPa geopotential height (solid white contoured every 60 m) at 1800 UTC 19 Dec 2009. (b) 13-km RUC analysis of MSLP (solid, contoured every 4 hPa), 1000–500 thickness (dashed, contoured every 60 m), and 250-hPa wind (shaded every 10 m s^{-1}) at 1800 UTC 19 Dec 2009. (c) As in (a), but at 0500 UTC 20 Dec 2009. (d) As in (b), but at 0500 UTC 20 Dec 2009.

observed crystals were classified following the 81 different types given by Magono and Lee (1966) and the different crystal types were then described in terms of the observed percentage fraction of ice habits within eight groups: needlelike, columns, dendritic, platelike, side planes, graupel, ice/miscellaneous, and sleet. Since the set of crystals within our samples usually displayed a range of riming, the degree of riming was quantified in terms of the observed lowest degree of riming, the mean degree of riming, and the highest degree of riming in the sample following Mosimann et al. (1994), ranging from a zero (no riming) to five (heavy riming). Because of the possibility of wind drift of precipitation particles aloft, we do not assume the observed habits form at the same time and location before reaching the surface.

3. The 19–20 December 2009 event

a. Synoptic evolution

On 19–20 December 2009 there was widespread heavy snowfall (27–70 cm) over Long Island, with 48.3 cm

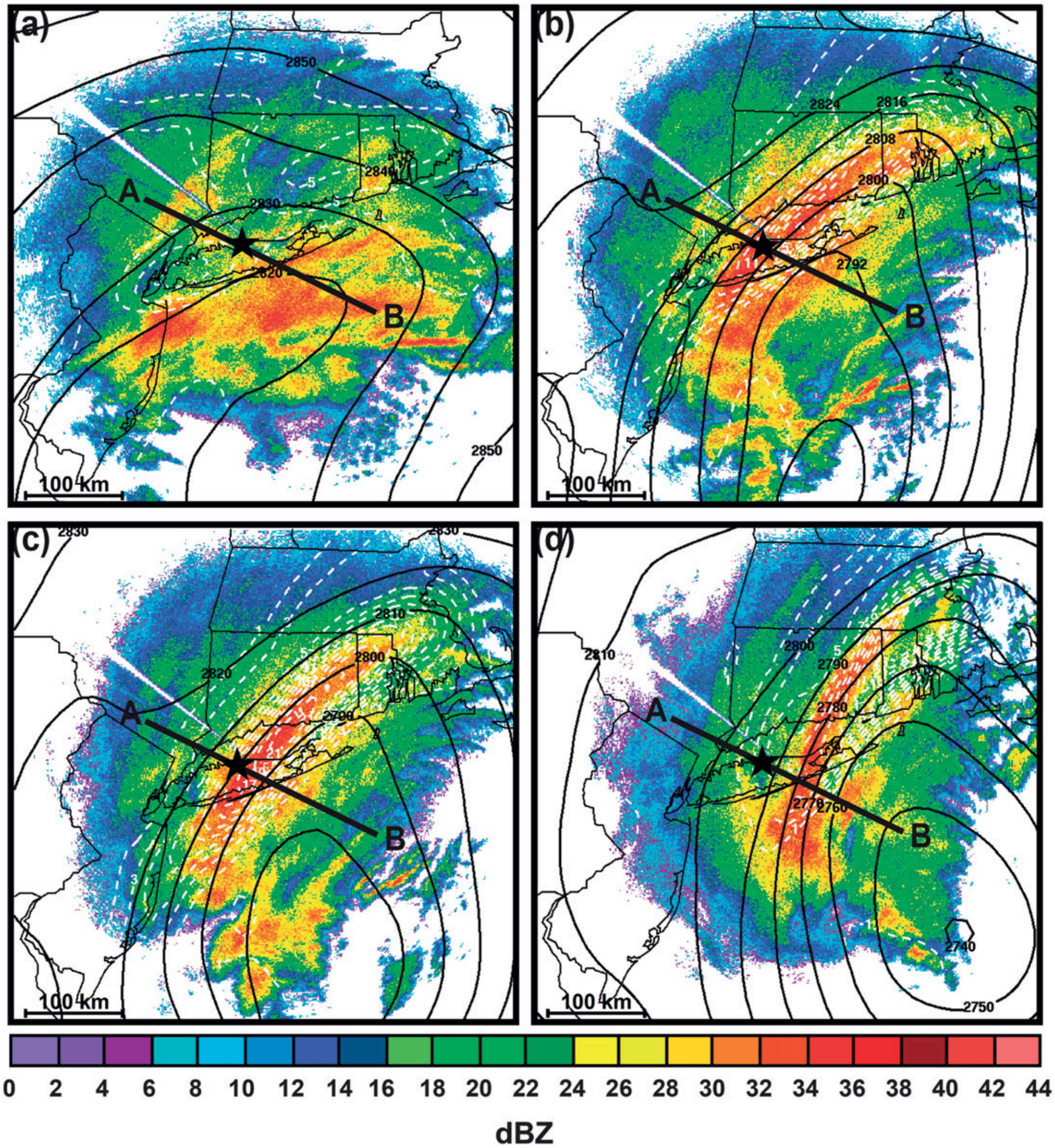

FIG. 3. KOKX WSR-88D radar reflectivity (color shaded every 2 dBZ starting at 0 dBZ) for the 2100 UTC 19 Dec 2009 simulation from the 13-km RUC showing 700-hPa geopotential height (solid, contoured every 10 m) and 700-hPa Miller 2D frontogenesis [positive values white dashed every 2 K $(100\ \mathrm{km})^{-1}\ \mathrm{h}^{-1}$] valid at (a) 0000 UTC, (b) 0400 UTC, (c) 0500 UTC, and (d) 0800 UTC 20 Dec 2009. The location of cross section AB is shown in each panel.

measured at SBNY (Fig. 1a). At 1800 UTC 19 December 2009, which is about 6 h before the heaviest snow began at SBNY, there was a broad 500-hPa trough across the eastern United States associated with a deepening cyclone (~988 hPa) located ~260 km to the northeast of Cape Hatteras, North Carolina (Fig. 2a). The surface cyclone low was centered near the left exit region of a 250-hPa jet streak (80–90 m s^{-1}) over North Carolina and Virginia (Fig. 2b). By 0600 UTC 20 December 2009, the surface cyclone (~984 hPa) was located ~280 km to the southeast of eastern Long Island (Fig. 2d), as a broad 500-hPa closed low was over the mid-Atlantic coast (Fig. 2c). Meanwhile, the New England region was under the comma head of the cyclone, while the midlevel dry air had wrapped around the closed low to near Cape Cod, Massachusetts.

b. Mesoscale evolution

At 0000 UTC 20 December 2009 (Fig. 3a), there was widespread snow across southern New England and Long Island, while a west–east precipitation band was developing ~60 km to the south of Long Island. This

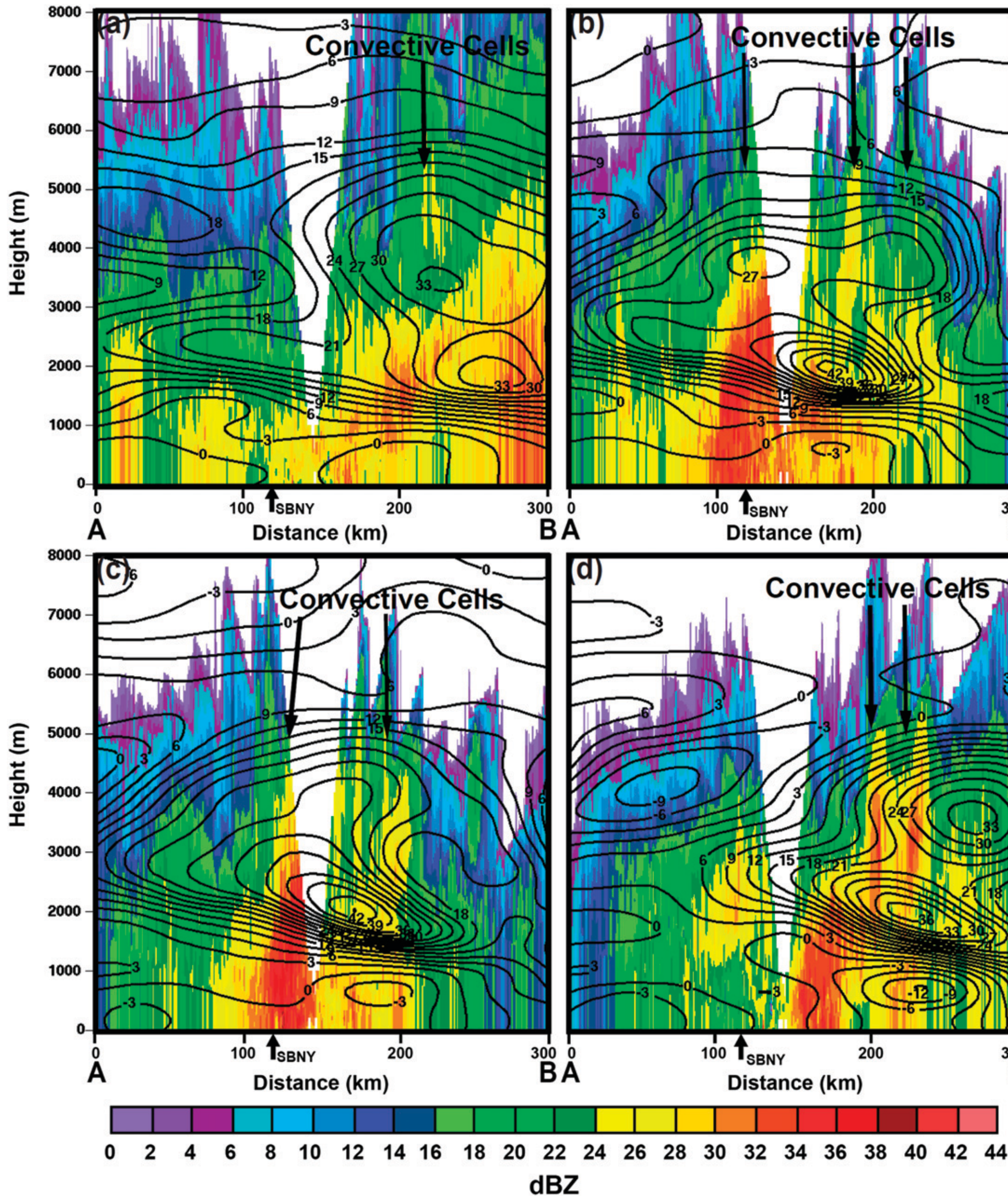

FIG. 4. Cross section AB showing KOKX WSR-88D radar reflectivity and vertical velocity (solid, contoured every 3 cm s^{-1}) for the 2100 UTC 19 Dec 2009 13-km RUC simulation valid at (a) 0000 UTC, (b) 0400 UTC, (c) 0500 UTC, and (d) 0800 UTC 20 Dec 2009. The location of section AB is shown in Fig. 3. SBNY represents Stony Brook, NY.

band was along a 700-hPa trough extending to the northeast of the parent low over southern New Jersey, with 700-hPa frontogenesis of 3–9 K $(100\ \mathrm{km})^{-1}\ \mathrm{h}^{-1}$ over Long Island. Cross section AB from SBNY to the southeast (Fig. 4a) shows a deepening area of precipitation to the south of Long Island in a northward-sloping region of ascent from 1.5 to 4 km MSL, with the strongest ascent (33 cm s^{-1}) closest to the developing band. Meanwhile, there were narrow convective cells above the developing band between 5 and 7 km MSL in a region of conditional instability, as illustrated by the area of negative saturation equivalent potential vorticity (EPV $= g\boldsymbol{\eta} \cdot \nabla\theta_{es}$, where g is gravity, $\boldsymbol{\eta}$ is the three-dimensional absolute vorticity vector, and $\nabla\theta_{es}$ is the three-dimensional gradient of the saturation equivalent potential temperature) and θ_{es} (saturation equivalent potential temperature) decreasing with height from 400 to 425 hPa (Fig. 5a). Across the southeastern portion of the vertical section, a layer of negative EPV exists from 700 to 800 hPa. However, θ_{es} is not decreasing with height in this region,

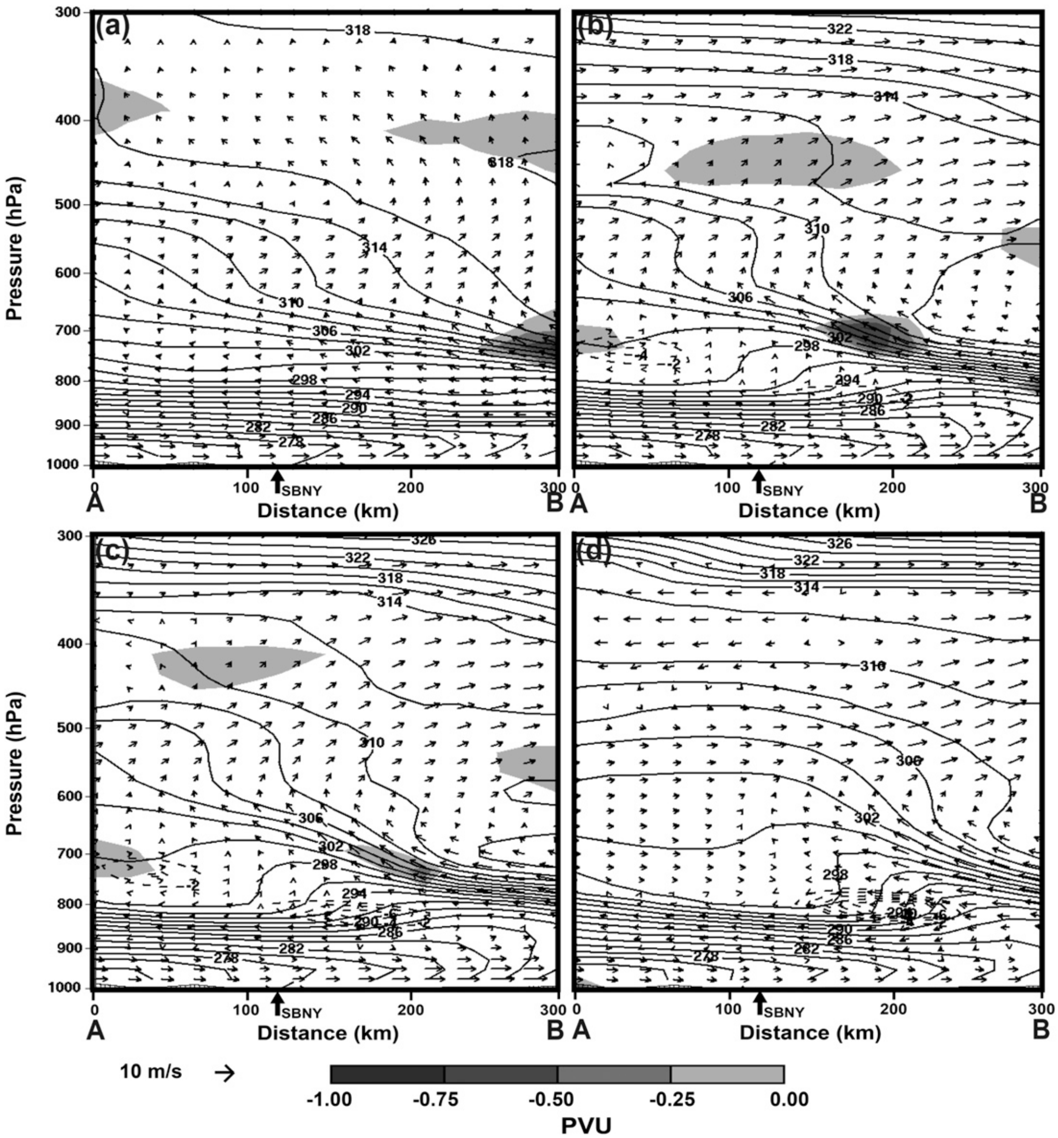

FIG. 5. Cross section AB from the 13-km RUC simulation starting at 2100 UTC 19 Dec 2009 showing saturation equivalent potential temperature (solid, contoured every 2 K), negative saturation equivalent potential vorticity (shaded where negative), negative absolute vorticity (black dotted every 2×10^{-5} s^{-1}), and circulation vectors (arrows) valid at (a) 0000 UTC, (b) 0400 UTC, (c) 0500 UTC, and (d) 0800 UTC 20 Dec 2009.

so there is likely conditional symmetric instability (Schultz and Schumacher 1999).

By 0400 UTC 20 December, the snowband intensified and was centered over central Long Island (33–38 dBZ) (Fig. 3b). Frontogenesis at 700 hPa increased to ~15 K (100 km)$^{-1}$ h^{-1} as the associated midlevel trough tightened just east of the heavy snowband (Fig. 3b). The vertical motion intensified to 42 cm s^{-1}, with the strongest reflectivities over SBNY (Fig. 4b). A region of conditional symmetric instability between 600 and 800 hPa was just southeast of SBNY, which likely helped enhance the frontogenetical circulation near and just above this layer (Fig. 5b). Between 800 and 825 hPa, absolute vorticity is negative, but this inertial instability is below the frontal ascent and most likely not contributing to the band development. Meanwhile, a layer of conditional instability still exists between 400 and 500 hPa, where θ_{es} decreases with height.

The snowband (33–38 dBZ) began moving to the east of SBNY at 0500 UTC 20 December 2009 (Figs. 3c and 4c), as the 700-hPa cyclone moved toward the northeast. There was little change in the strength or positioning of the strongest vertical motion in section AB during the past few hours (Figs. 4b,c). The conditional symmetric

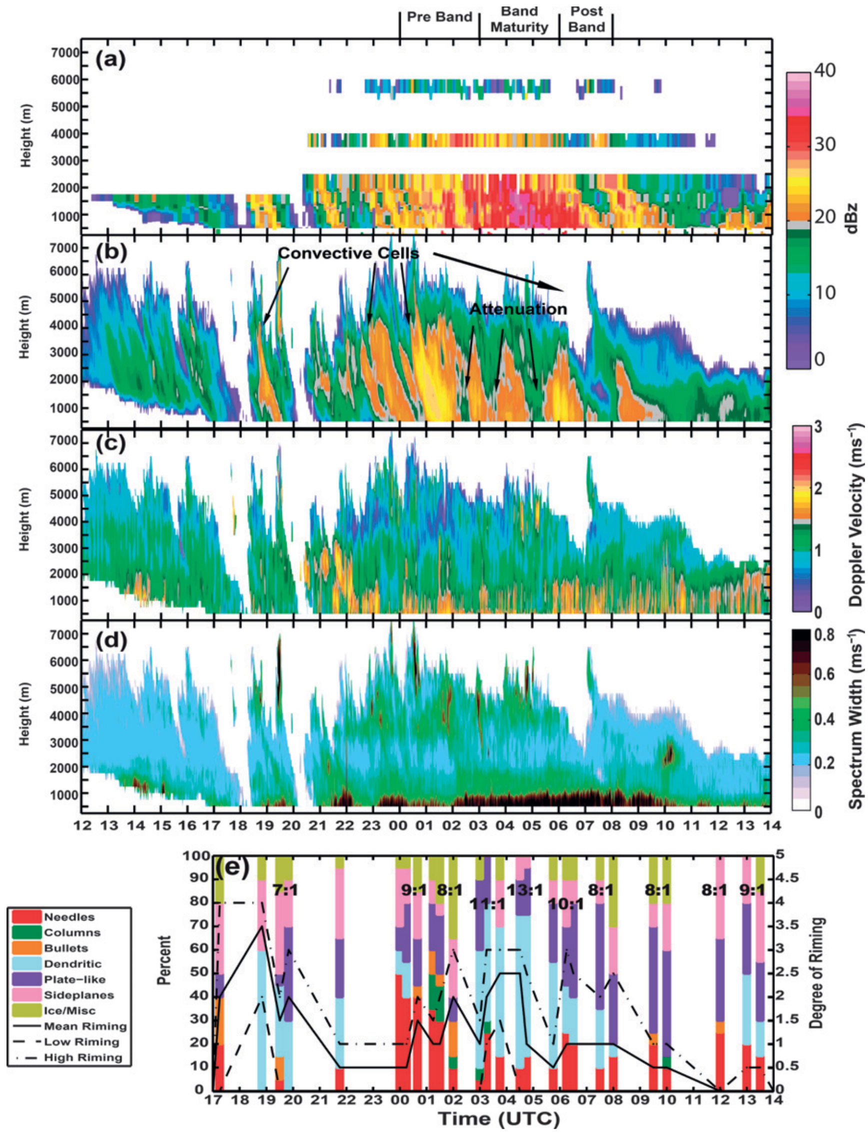

FIG. 6. (a) KOKX radar reflectivity (shaded in dBZ), (b) MRR radar reflectivity (shaded in dBZ), (c) MRR Doppler vertical motion (shaded in m s^{-1}), and (d) MRR spectral width (m s^{-1}) time–height between 1200 UTC 19 Dec and 1400 UTC 20 Dec 2009. (e) Field observations of the microphysical evolution of ice habit (shaded vertical bars), riming (mean: solid, low: dashed, high: dotted–dashed), and snow-to-liquid ratio (labeled) from 1700 UTC 19 Dec to 1400 UTC 20 Dec 2009.

instability between 600 and 700 hPa associated with this band decreased slightly in intensity, while the conditional instability aloft continued to support the convective cell growth (Fig. 4c).

By 0800 UTC 20 December, the heavy snowband was located across eastern Long Island, with light to moderate snowfall occurring over SBNY (Fig. 3d). The 700-hPa trough had moved ~150 km east of SBNY, with the strongest 700-hPa frontogenesis on the western side of the trough continuing to support the band (Fig. 3d). There were still convective cells aloft as depicted in the reflectivity cross section (Fig. 4d), but there was no negative EPV aloft at this time, which may be the result of the RUC stabilizing the atmosphere too quickly (Fig. 5d).

c. Microphysical evolution

Figure 6 shows a time–height section of OKX radar reflectivity and MRR radar reflectivity, MRR Doppler velocity, and MRR spectral width over SBNY from 1200 UTC 19 December to 1400 UTC 20 December

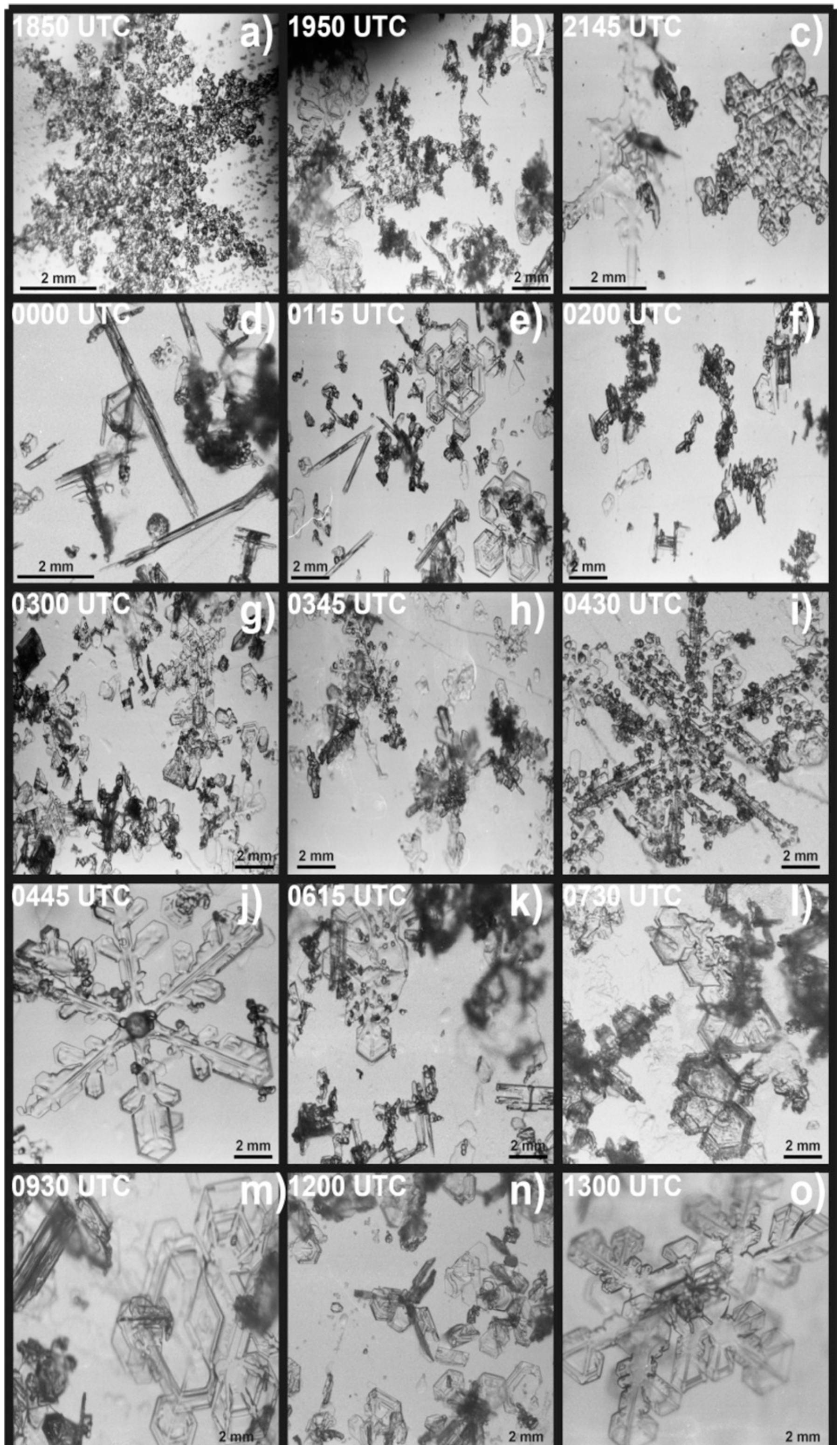

FIG. 7. Observed snow habit pictures using a stereo microscope during the 19–20 Dec 2009 heavy snowband event. (a)–(c) Occurred on 19 Dec 2009. Some of the crystals are not lying flat and the time represents when crystals were observed.

2009. The surface evolution of the ice habit, riming, and snow-to-liquid ratio at SBNY is also shown from 1700 UTC 19 December to 1400 UTC 20 December 2009 (Fig. 6e). Between 1500 and 2000 UTC 19 December, there were several convective cells above 3.5 km MSL. The precipitation with these cells extended to the surface in fall streaks detected by the MRR (Fig. 6b) and in the OKX time height (Fig. 6a). Evidence for these generating cells above 3.5 km AGL are intermittent higher reflectivity values, higher spectral widths (>0.35 m s^{-1}) indicating more turbulence, and lower Doppler velocities (less than ~0.7 m s^{-1}, fall velocity of snow particles is partially offset by upward air motions). These cells aloft were likely acting as the seeder portion of a "seeder–feeder" process (Hill et al. 1981; Rutledge and Hobbs 1983). When the precipitation aloft from the first of these cells descended to the surface starting at 1700 UTC 19 December, bullets (~20%), side planes (~30%), and a few platelike (~10%) habits were observed with an average degree of riming of 2. Moderate to heavily rimed dendritic crystals (Fig. 7a) were common (~60%) at 1845 UTC. By 1930 UTC, the dendritic crystals decreased to ~30%, there were more side planes (~35%) and bullets (~10%), and the mean degree of riming decreased from 3.5 to 1.5 (Fig. 7b). As the initial group of generating cells finished passing over SBNY at 1945 UTC, there were more moderately rimed platelike crystals (~40%) (Fig. 7c). The snow-to-liquid ratio was 7:1 during the period of 1900–2000 UTC (Fig. 6d).

1) PRESNOWBAND (0000–0300 UTC)

During the few hours before the heavy snowband reached SBNY, the tallest precipitation echo tops (~30-dBZ echo) in the MRR increased to ~7 km MSL as additional convective cells moved overhead. Radar reflectivities from KOKX were generally 25–30 dBZ. The MRR radar reflectivities were within a few dB of those from KOKX until about 0130 UTC when wet snow began to accumulate on the dish and attenuated the signal to varying degrees (the annotation in Fig. 6b indicates periods of particularly strong attenuation). Nearly 40% of the observed crystals were needlelike from 0000 to 0200 UTC with light riming (Figs. 7d,e), but as the precipitation intensified from 0100 to 0300 UTC (Fig. 6), the mean degree of riming increased to 2 and bullets (Fig. 7d), columns (Fig. 7e), side planes (Figs. 7e,f), and some plates (Fig. 7e) were observed.

The changes in the degree of riming observed at the surface with time are indirectly seen in the profiles of Doppler velocity within the layer below the generating cells where $\sigma < 0.5$ m s^{-1} (Figs. 6c,d,e and 8). Overall, these profiles show a general trend of increasing Doppler velocity with decreasing height, consistent with growth as

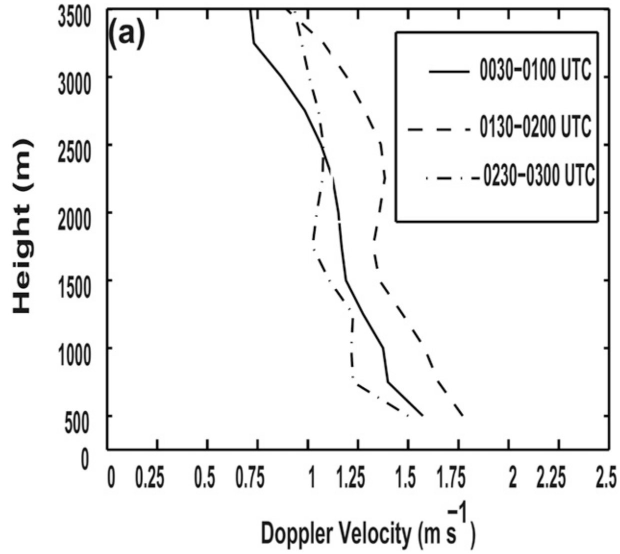

FIG. 8. Average vertical MRR Doppler velocity (m s^{-1}) profiles for the preband period during the 19–20 Dec 2009 snowband event. The time period used to calculate each profile is given in the legend.

the particles fall. In the absence of other sources of upward motions, shifts in the profiles to higher Doppler velocity values correspond to periods of higher fall speeds and higher degrees of riming. For example, from 0030 to 0100 UTC, the Doppler velocities increased from 0.7 m s^{-1} at 3.5 km MSL to 1.25 m s^{-1} at 1.25 km MSL as the snow crystals grew and become more rimed, more dense, and had higher fall speeds at lower levels. Below ~1-km altitude, spectral width values >0.5 m s^{-1} indicate likely contributions from boundary layer turbulence. During the period from 0130 to 0200 UTC when the degree of mean riming increased to 2, the Doppler velocity profile below 3.5 km MSL altitude shifted to values from about 0.1 to 0.25 m s^{-1} higher than those during period from 0030 to 0100 UTC (Fig. 8). By 0200 UTC 20 December, the proportion of needlelike crystals decreased to 10% with more ice/miscellaneous (~35%), ~25% side planes, ~15% bullets, ~10% platelike, and ~5% columns (Fig. 7f). In the period from 0230 to 0300 UTC, the degree of riming decreased to 1 and the MRR Doppler velocity profile shifted back to lower values below 3.5-km altitude. (Fig. 8). The snow-to-liquid ratio was ~8.5:1 from 0000 to 0300 UTC (Fig. 6d).

The vertical air motion profile from the RUC at 0000 UTC 20 December 2009 has maximum ascent (22 cm s^{-1}) at ~690 hPa (~2.9 km MSL) (Fig. 9c). The layer between 680 and 850 hPa (~2.8 km and 1.3 km MSL) contains an RH$_{(\mathrm{water})}$ of nearly 100% (Fig. 9a) and an RH$_{(\mathrm{ice})}$ of ~105% (Fig. 9b). This layer has temperatures between −5° and −10°C (Fig. 9d), thus favoring needle growth (Magono and Lee 1966, see their Fig. 2;

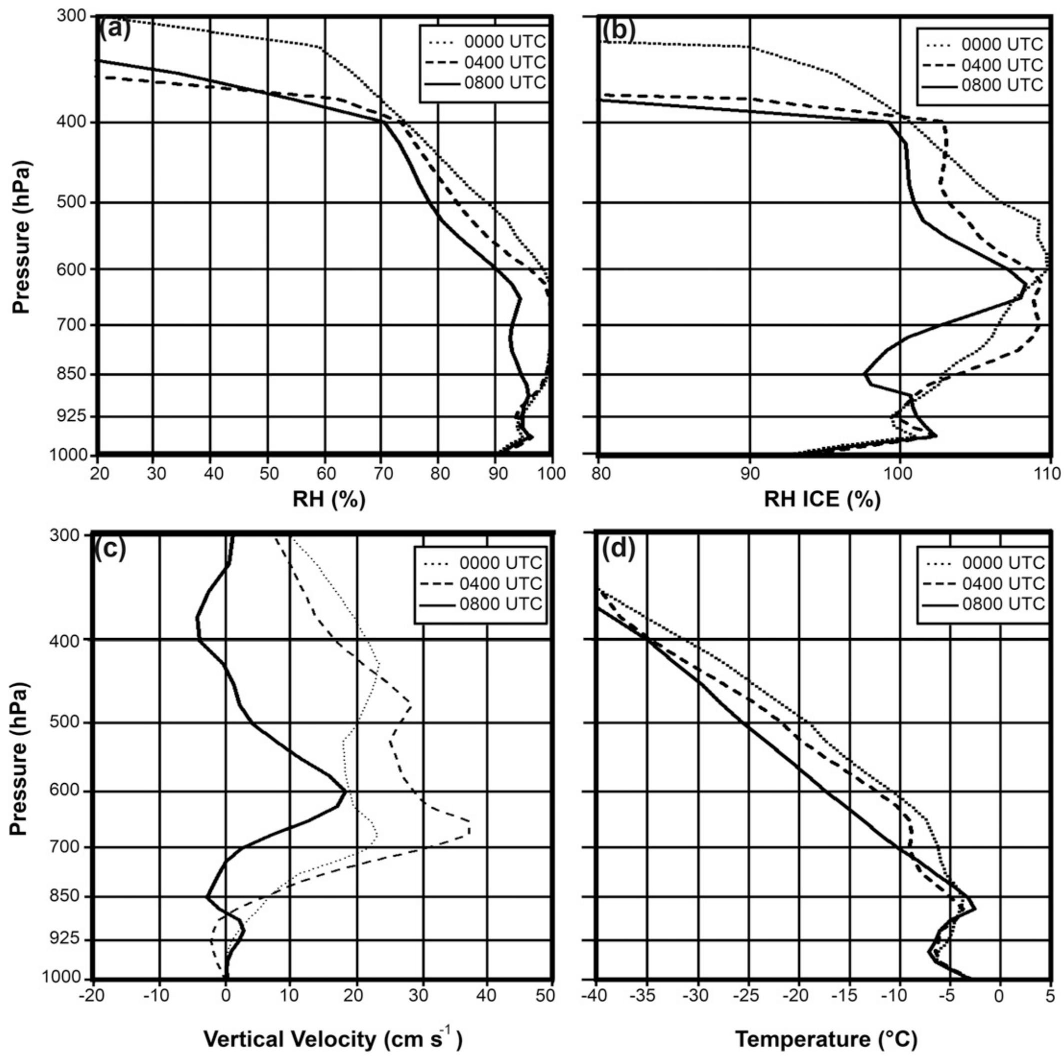

FIG. 9. Vertical profiles of (a) relative humidity with respect to water (%), (b) relative humidity with respect to ice (%), (c) vertical velocity (cm s^{-1}), and (d) temperature (°C) from the 2100 UTC 19 Dec 2009 run of the 13-km RUC. The dotted, dashed, and solid lines are for the 0000 UTC, 0400 UTC, and 0800 UTC 20 Dec 2009 times, respectively.

Hobbs 1975, see his Table 2; Stoelinga et al. 2007, see their Fig. 5; Bailey and Hallett 2009, see their Fig. 5), which was the dominant surface habit. The RUC showed no significant change in the temperatures between 0000 and 0300 UTC from 600 to 700 hPa (~4 km to 3 km MSL) as the maximum ascent continued in this layer (not shown). Some of the colder crystal types observed (side planes, columns, and bullets) during the preband period were most likely formed in seeder cells aloft, where temperatures were colder than −20°C between 400 and 500 hPa.

2) SNOWBAND MATURITY (0300–0600 UTC)

During the first 45 min of band maturity (0300–0345 UTC), the observed ice habit was 50%–55% dendritic (Figs. 6d and 7h). There were ~30% platelike habits at 0300 UTC (Fig. 7g) that decreased to ~20% by 0315 UTC and eventually zero by 0345 UTC as the dendritic crystals became the dominant habit. The remaining observed crystals between 0300 and 0345 UTC were ~15% needles, ~7% side planes, ~7% ice/miscellaneous, and ~3% columns. Between 0300 and 0345 UTC, the mean degree of riming increased from 1 to 2.5, with some dendritic crystals more heavily rimed (Fig. 7i). About 65% of the crystals were dendritic between 0345 and 0430 UTC and the degree of riming remained near 2.5. The OKX time height from 0300 to 0430 UTC showed an increase in reflectivity from 35 to 40 dBZ as the riming increased (Fig. 6a). Associated with the increased proportion of dendritic snow crystals was an increase in snow-to-liquid ratios to 11:1 (Fig. 6b). The vertical

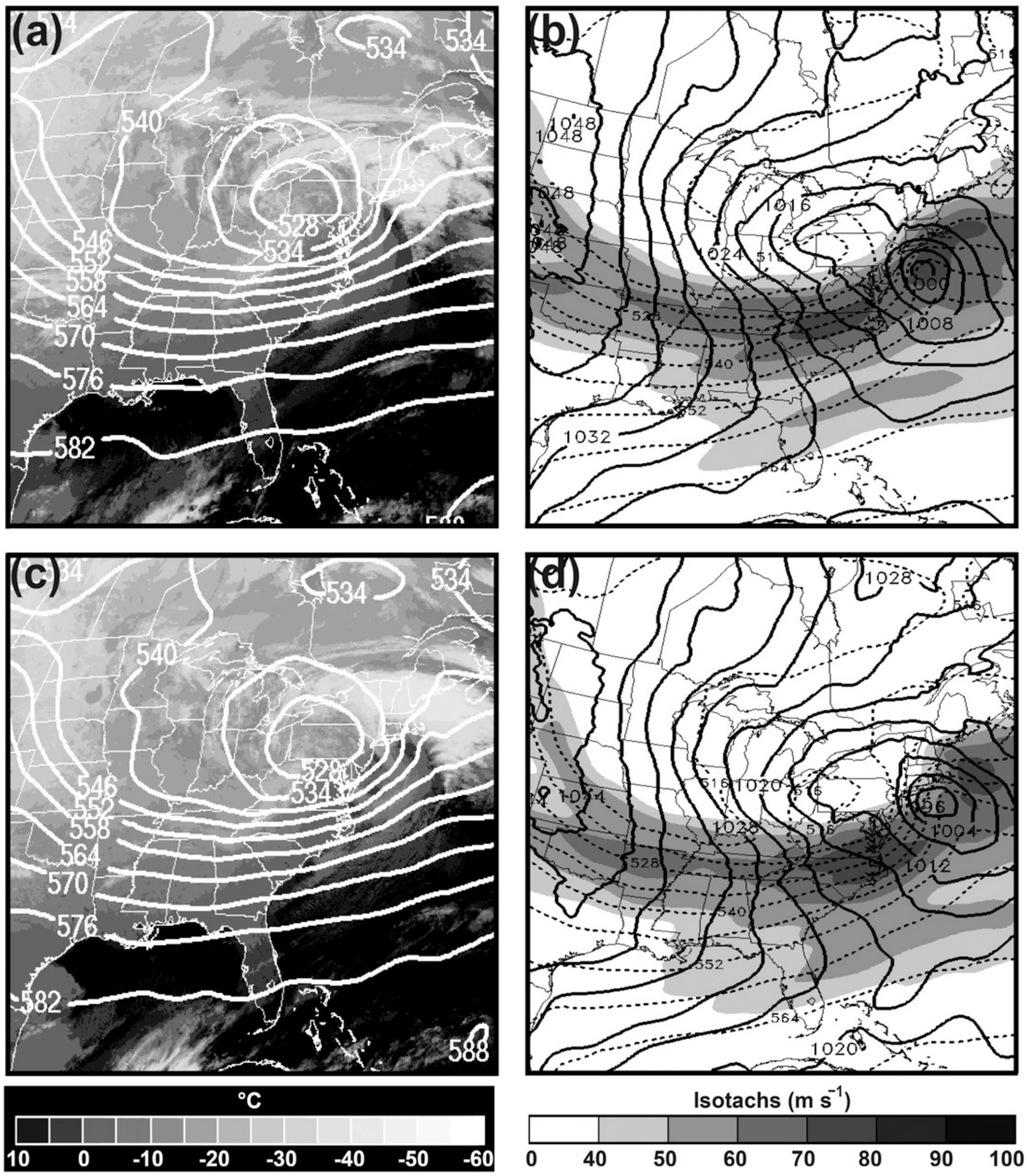

FIG. 10. (a) *GOES-13* infrared satellite brightness temperature (°C, shaded), 12-km NAM analysis of 500-hPa geopotential height (solid white, contoured every 60 m) and 500-hPa wind (full barb = 10 m s^{-1}, pennant = 25 m s^{-1}) at 0600 UTC 12 Jan 2011. (b) 12-km NAM analysis of MSLP (solid, contoured every 4 hPa), 1000–500 thickness (dashed every 60 m), and 250-hPa wind (shaded every 10 m s^{-1}) at 0600 UTC 12 Jan 2011. (c) As in (a), but 12-km NAM 3-h forecast from 0600 UTC cycle at 0900 UTC 12 Jan 2011. (d) As in (b), but 12-km NAM 3-h forecast from 0600 UTC cycle at 0900 UTC 12 Jan 2011.

motion profile from the RUC at 0400 UTC is supportive of dendritic growth indicating a vertical motion maximum (~37 cm s^{-1}) between 600 and 700 hPa (Fig. 9c). The temperatures in this layer, which had been −6° to −9°C at 0000 UTC, cooled to −12° to −15°C by 0400 UTC (Fig. 9d). The reason for this cooling between 0200 and 0400 UTC was explored using the RUC 5–7-h forecast at 650–750 hPa by calculating the horizontal and vertical temperature advections, adiabatic, and diabatic term (diabatic calculated as a residual from the local hourly temperature change and the other thermodynamic terms). There was weak warm advection and significant diabatic (latent) heating, but there was net cooling during this period from adiabatic ascent (not shown). This layer also continued to have 100% $RH_{(water)}$ (Fig. 9a), but $RH_{(ice)}$ increased to ~109% (Fig. 9b).

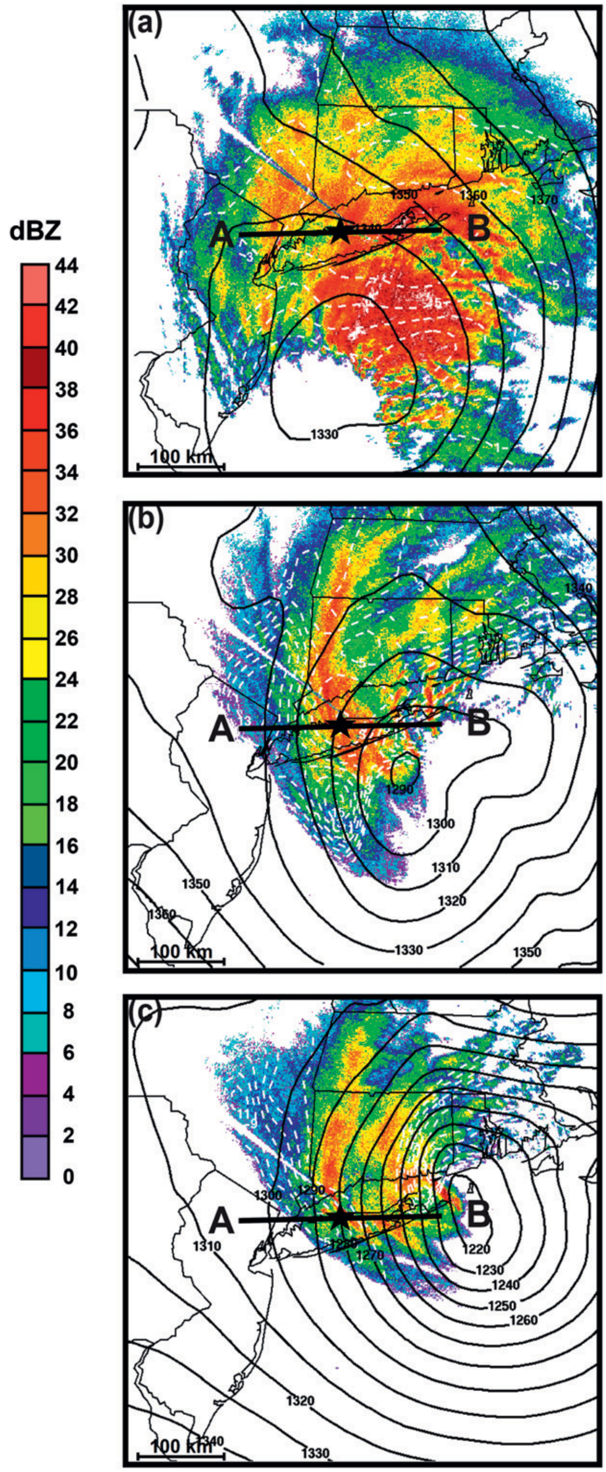

FIG. 11. (a) As in Fig. 3, but for the 0600 UTC 12 Jan 2012 simulation of the 12-km NAM showing 850-hPa geopotential height (solid every 30 m) and 850-hPa Miller 2D frontogenesis [white dashed every 2 K $(100\ \mathrm{km})^{-1}\ \mathrm{h}^{-1}$] valid at 0600 UTC 12 Jan 2011. (b) As in (a), but valid at 0000 UTC 12 Jan 2011. (c) As in (a), but valid at 1200 UTC 12 Jan 2011. The location of cross section AB for Fig. 12 is shown in each panel.

As the western portion of the snowband crossed SBNY, the degree of riming rapidly decreased from 3 at 0430 UTC to 1 at 0445 UTC (Fig. 6d). Dendrites remained the primary snow habit during this riming decrease (Fig. 7j). We hypothesize that the riming was largest on the east side of the band, since the strongest frontogentical forcing and ascent was concentrated on the warm (east) side of the midlevel baroclinic zone (Figs. 4c and 5c). The riming decreased on the west side of the band as the weaker upward motion did not create as much supercooled water, since the $\mathrm{RH}_{(\mathrm{water})}$ decreased from near 100% at 0400 UTC to 95% at 0600 UTC (not shown). Coinciding with this period of decreased riming, the snow-to-liquid ratios increased to 13:1 (Fig. 6e).

3) POSTSNOWBAND (0600–0800 UTC)

The precipitation became less intense (25–30 dBZ) as the snowband moved to the east of SBNY (Fig. 6a). There was a decrease in vertical motion aloft after 0600 UTC, and by 0800 UTC the ascent at ~600 hPa was from 10 to 20 cm s^{-1}. This weaker ascent was located in a layer between $-15°$ and $-20°\mathrm{C}$ (Figs. 9c,d), and an $\mathrm{RH}_{(\mathrm{water})}$ of ~90% (Fig. 9a), which is supportive of the more platelike crystals observed in this period (Fig. 6e). Between 0600 and 0745 UTC (Fig. 6d), plates increased from 25% to 45% (Figs. 7k,l), while the dendritic habits decreased from 45% to 20%. The remaining crystals were needles (~20%), side planes (~10%) and ice/miscellaneous (~5%). Although a few platelike (Fig. 7l) and ice/miscellaneous (Fig. 7l) were moderately rimed, from 0600 to 0800 UTC 20 December was characterized by an average degree of riming of 1. As more plates were observed, the snow-to-liquid ratios slowly decreased from 13:1 to 11:0 between 0500 and 0630 UTC (Fig. 6d), and further decreased to 8:1 between 0630 and 0800 UTC (Fig. 6d).

After a lull in the precipitation at SBNY between 0700 and 0800 UTC (Figs. 6a,b), particles from another convective cell aloft at 0700 UTC descended to the surface between 0800 and 0900 UTC. Overall, the ice habit remained platelike (Figs. 6d and 7m). The echo tops rapidly decreased to 4 km MSL after this cell moved east (Fig. 6b), and the degree of riming slowly decreased to zero by the end of the event with main ice habits including plates (~40%), side planes (~25%), needles (~20%), and dendrites (~10%) (Figs. 7m,n,o). The snow-to-liquid ratio remained near 8:1 during this period (Fig. 6d).

4. 12 January 2011

The goal of this section is to highlight the microphysical evolution of a snowband event that occurred with a coastal

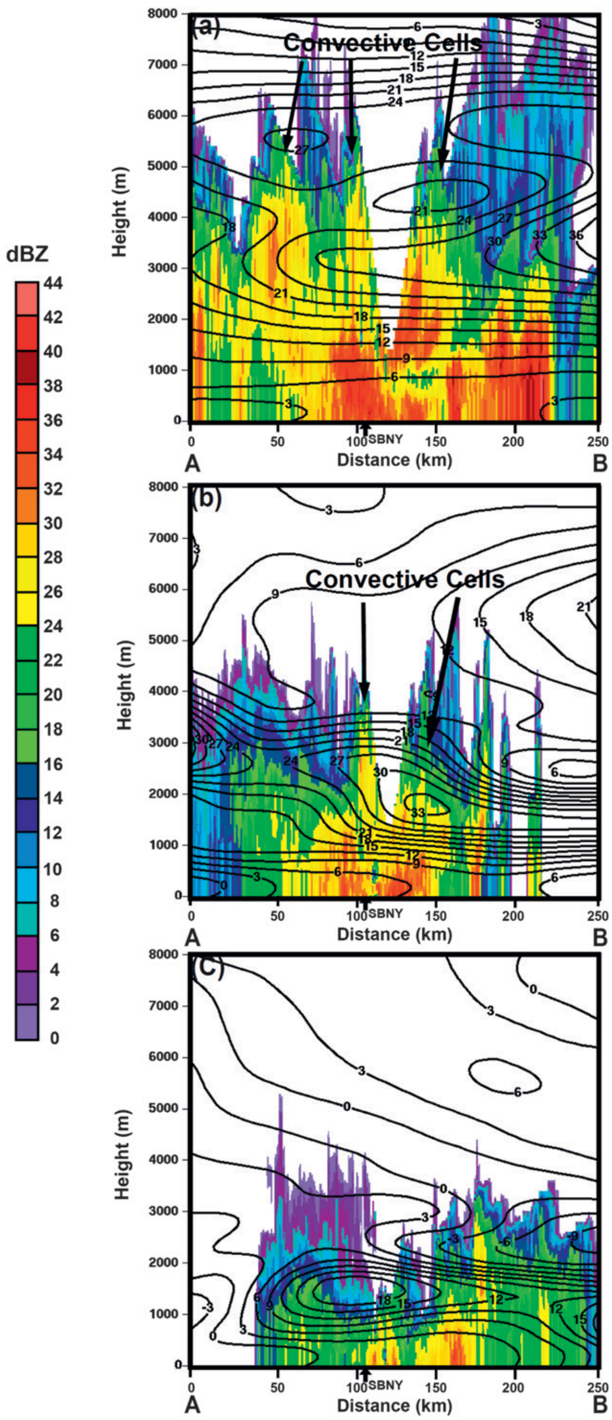

FIG. 12. Cross section AB of the KOKX WSR-88D radar reflectivity and vertical velocity (solid, contoured every 3 cm s^{-1}) for the 0600 UTC 12 Jan 2011 simulation of the 12-km NAM valid at (a) 0600 UTC, (b) 1000 UTC, and (c) 1200 UTC 12 Jan 2011. The location of section AB is in Fig. 11. SBNY represents Stony Brook, NY.

cyclone on 12 January 2011, which resulted in ~41 cm of snow at SBNY (Fig. 1b), so it can be compared with the microphysical evolution on 19–20 December 2009.

a. Synoptic and mesoscale overview

At 0600 UTC 12 January 2011, a surface cyclone (~1000 hPa) was developing ~230 km south of Long Island under a 70–80 m s^{-1} jet at 250 hPa (Fig. 10b.), while a closed 500-hPa low was centered over the southeastern Great Lakes (Fig. 10a). The coldest cloud tops (from about −40° to −50°C) were across eastern Long Island and to the north and east. Warmer cloud tops (from about −5° to −15°C) were to the south of Long Island with the approach of a midlevel dry intrusion (Fig. 10a). By 0900 UTC 12 January 2011, the midlevel dry air had moved northeastward to western Long Island (Fig. 10c). The cyclone intensified to ~996 hPa and was located ~82 km southeast of Long Island in the left exit region of the southern jet core (Fig. 10d).

At 0600 UTC 12 January, heavy snow developed across eastern New Jersey and southeast New York, while the dry intrusion was situated just east of the southern New Jersey coast (Fig. 11a). The strongest frontogenesis was at 850 hPa, which extended to the north and east of an 850-hPa closed circulation situated about 160 km to the south of Long Island. Cross section AB illustrates moderate to heavy precipitation (25–35 dBZ) throughout the section from the surface up to 3.5 km MSL. The strongest vertical velocities (>30 cm s^{-1}) are located over the southeast portion of the cross section at 3 km MSL. There are also convective cells from 3 to 6 km MSL. Upward motion (30–33 cm s^{-1}) between 5 and 6 km combined with conditional instability (Fig. 12a), where moist EPV is less than zero in a region with θ_{es} decreasing with height, supported these cells. The moist EPV is also less than zero between 750 and 850 hPa (~2.5–1.3 km MSL) over the southeast portion of section AB (Fig. 12a), and there is no θ_{es} decrease with height, which suggests a region of conditional symmetric instability (Fig. 13a). The western portion (0–50 km) of this section from 550 to 600 hPa (~4.5–4.0 km MSL) has some inertial instability, where the negative absolute vorticity and moist EPV are less than zero (Fig. 13a).

The 850-hPa low moved north and was located ~95 km south of SBNY at 1000 UTC (Fig. 11b.). The inverted trough to the north of the 850-hPa low amplified, with the strongest frontogenesis located ~100 km to the north and west of this trough. The primary heavy snowband extended from central Massachusetts to central Long Island, while there were a few smaller bands over eastern Long Island. Meanwhile, the drier air was located across the eastern half of cross section AB (Fig. 12b). A maximum in upward motion extended from 1.5 km MSL just

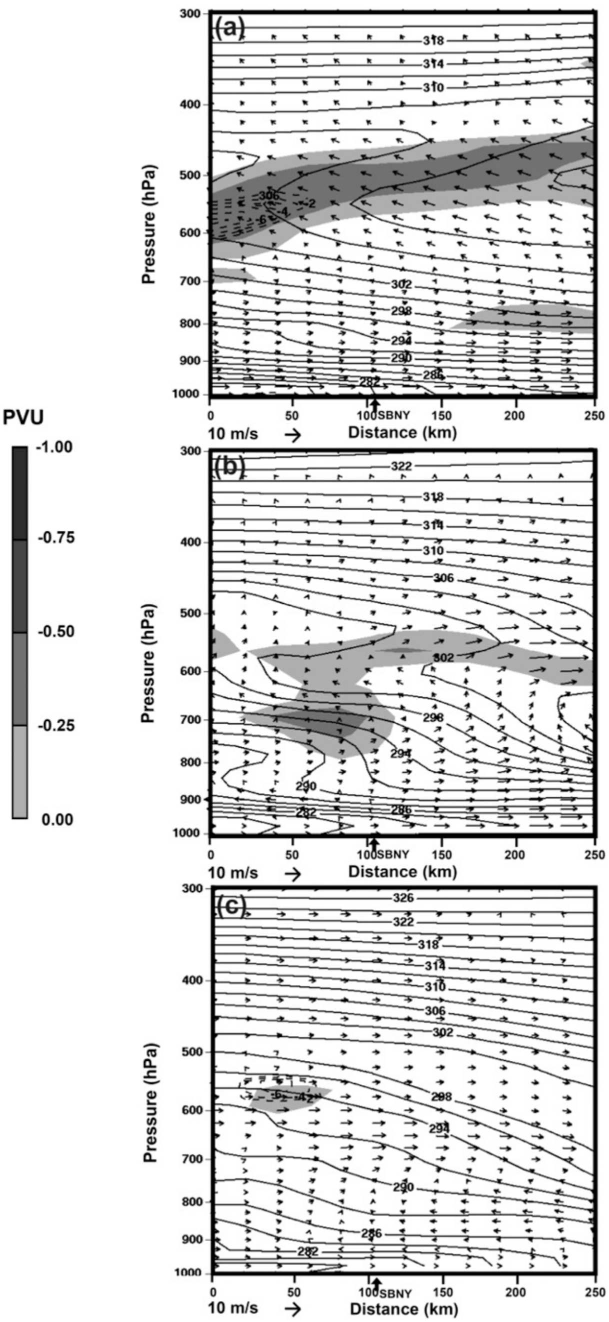

FIG. 13. As in Fig. 5, but using the 0600 UTC 12 Jan 2011 simulation from the 12-km NAM valid at (a) 0600 UTC, (b) 1000 UTC, and (c) 1200 UTC 12 Jan 2011.

east of SBNY to 3 km over the snowband, with values approaching 30–33 cm s^{-1}. Conditional instability was still present from 500 to 600 hPa (~5.4– 4.0 km MSL) (Fig. 13b) and between 650 and 750 hPa (~3.5–2.5 km MSL) across the western portion of the cross section in support of the heavy snowband. The frontogenetical circulation is evident in Fig. 13b, but it is relatively weak, which may be the result of the 12-km NAM not capturing the intensity of this event.

The snowband began weakening by 1200 UTC 12 January as it moved east of SBNY. The 850-hPa low was near the eastern tip of Long Island and the inverted trough to the north broadened and frontogenesis weakened (Fig. 11c.). Cross section AB at 1200 UTC showed a decrease in magnitude of vertical velocity (maximum near 18 cm s^{-1}), and a decrease in the height of the band (Fig. 12c). The environment surrounding the band began to stabilize, as the negative moist EPV was limited to 550–600 hPa (~4.5–4.0 km MSL) across the western portion of section AB (Fig. 13c). Most of this negative EPV was in a region of negative absolute vorticity indicating inertial instability. The frontogenetical circulation also weakened by 1200 UTC 12 January (Fig. 13c).

b. *Microphysical evolution*

1) PRESNOWBAND (0600–1000 UTC)

Between 0600 and 0700 UTC, the MRR observed several convective cells between 3 and 6 km MSL (Figs. 14a–d). The observed snow habits (Fig. 14d) were needles (~47%), dendrites (~27%; Figs. 15a,b), columns (~18%; Fig. 15c), plates (~7%), and ice/miscellaneous (~2%). The average degree of riming ranged from 1 to 3, but some dendritic crystals were heavily rimed (>4) at 0600 UTC (Fig. 15b). MRR Doppler velocities between 0600 and 0700 UTC increased with decreasing height from 0.25 m s^{-1} at 2.5 km to 1.5 m s^{-1} at 1 km (Fig. 16a). The snow-to-liquid ratio was ~8:1 between 0600 and 0700 UTC (Fig. 14d).

Between 0700 and 0800 UTC, ice habits (Fig. 14d) consisted of needles (~45%; Fig. 15e), columns (~40%; Fig. 15d), and a small amount of graupel (~10%; Fig. 15f). Both OKX and the MRR indicated a several km decrease in 15-dB*Z* echo-top height over SBNY between 0700 and 0830 UTC (Figs. 14a,b) associated with drier air moving over SBNY. Subsequent to the dry slot, the MRR indicated strong turbulence within the snow echo from 0830 to 0950 UTC. The slanting patterns in the time–height plots of Doppler velocity and spectral width indicate two turbulent layers that increased in height with time. A top layer with strong upward motions (small positive Doppler velocities) overlying strong downward motions (large positive Doppler velocities). The surface microphysical observations made just before 0900 UTC, when the MRR reflectivities, downward velocities, and spectral width reached their peak values during the storm, included a large quantity of lump graupel (45%) as well as heavily rimed needles and columns (Figs. 14d and 15g). Between 0930 and 1000 UTC, no graupel was observed and needlelike crystals (Fig. 15g) became

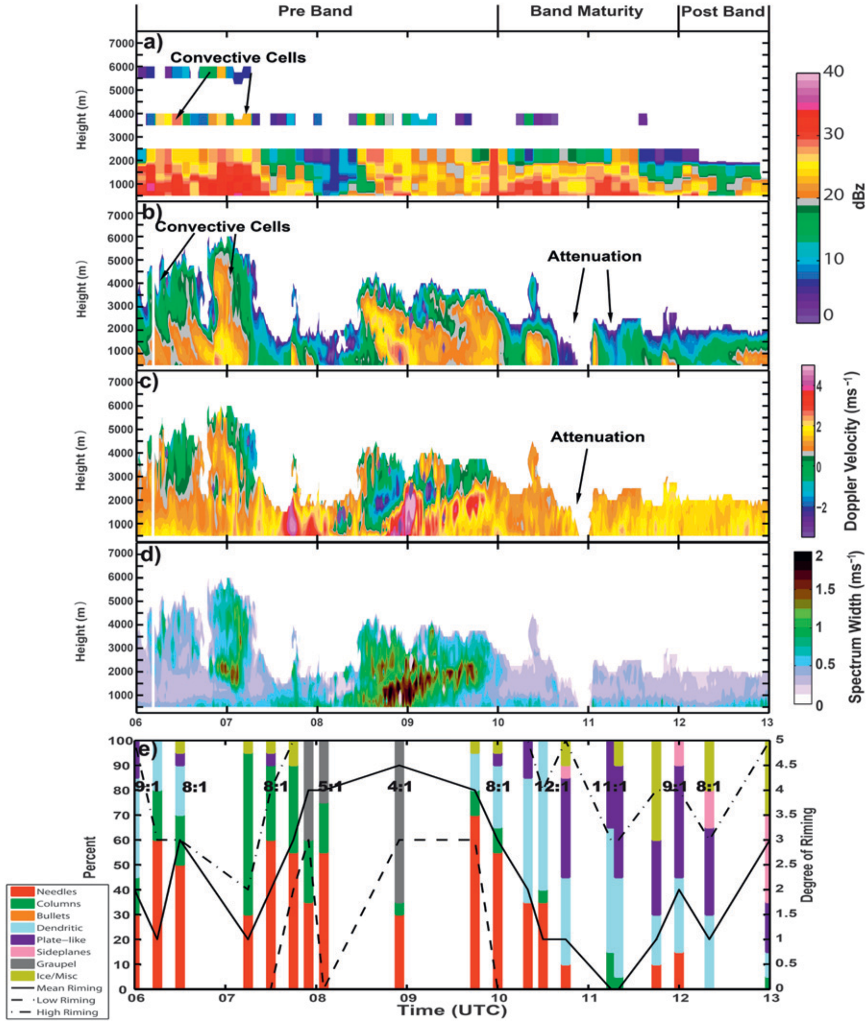

FIG. 14. As in Fig. 6, but from the 12 Jan 2011 event.

dominant (~70%) The associated MRR Doppler velocity profile showed higher values (~2.5 m s^{-1}) near 2 km MSL altitude where spectral width was also high (>1 m s^{-1}) and lower values near the surface (1.5 m s^{-1}) where spectral width was lower. This pattern indicates that the snow particles formed in the generating cells aloft had strong enough horizontal motions to not fall directly downward (i.e., that the snow near the surface did not originate directly overhead). The snow-to-liquid ratio decreased from 8:1 at 0730 UTC to 5:1 by 0800 UTC and was as low as 4:1 during the graupel period near 0900 UTC (Fig. 14e). Within the main snowband at 1000 UTC the snow-to-liquid ratio was 8:1 (Fig. 14e).

Based on the NAM vertical profiles, the maximum upward motion (20–30 cm s^{-1}) during the preband period occurred between 500 and 700 hPa (~5.4–3.0 km MSL; Fig. 17c) within temperatures from −5° to −10°C (Fig. 17d), which helped support the growth of needles. Near 100% $RH_{(water)}$ was present between 675 and 900 hPa (~3.3–1.0 km MSL; Fig. 17a) and the $RH_{(ice)}$ was between 103% and 108% (Fig. 17b). The NAM does not capture the small-scale strong upward motions associated with the observed graupel production.

2) SNOWBAND MATURITY (1000–1200 UTC)

At 1000 UTC, the snowband was over SBNY (Figs. 14a,b). The maximum upward motion (28–31 cm s^{-1}) at SBNY was now between 600 and 800 hPa (~4.0–2.0 km MSL) (Fig. 17c), where the temperatures were −9° to −10°C (Fig. 17b). A thermodynamic budget in this layer from the RUC revealed that the temperatures cooled by ~3°C primarily from adiabatic cooling (not shown). $RH_{(water)}$ was near 100% in this layer, and $RH_{(ice)}$ was between 105% and 115%. These factors led to more dendrites (~40%) being observed (Figs. 15h,j) and fewer needles (~20%) than during the preband

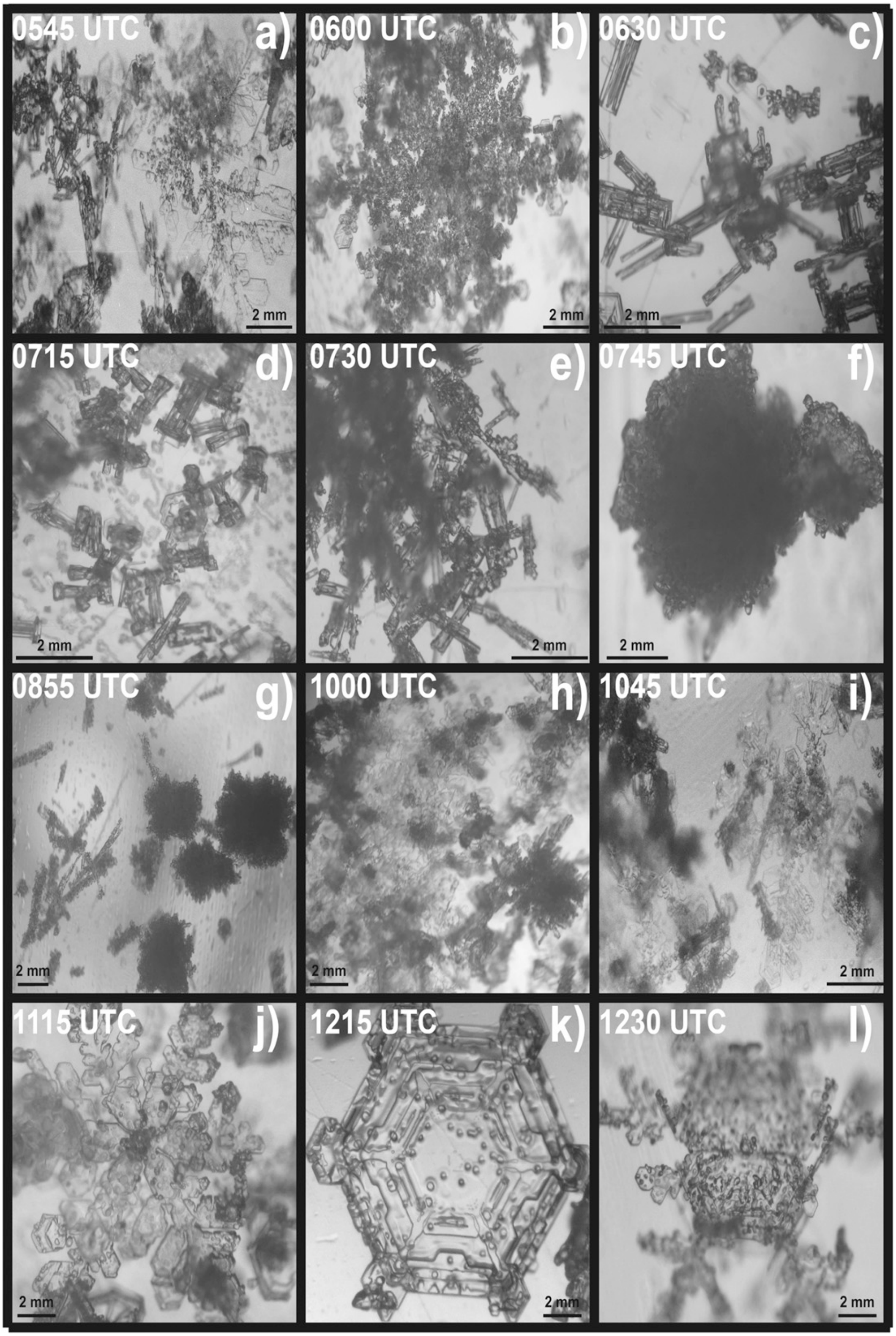

FIG. 15. As in Fig. 7, but for ice habit pictures from the 12 Jan 2011 event.

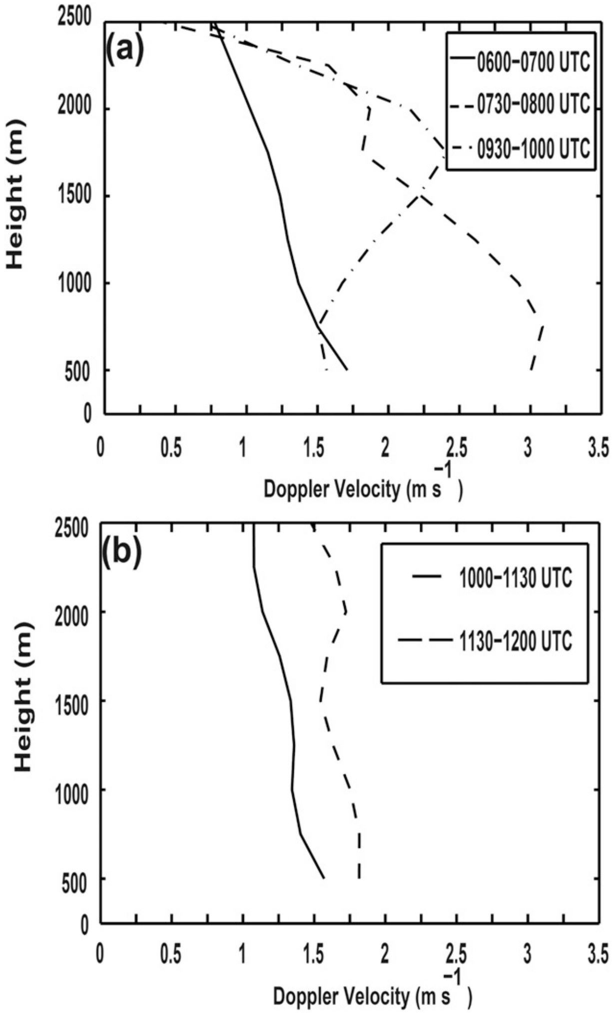

FIG. 16. As in Fig. 8, but for the 12 Jan 2011 snowband event from (a) 0600 to 1000 and from (b) 1000 to 1200 UTC 12 Jan 2011.

period (Figs. 15h,j). The average riming factor decreased from 3 at 1000 UTC to 1 by 1030 UTC. The radar echo was shallower, 15-dBZ echo tops were <2.5 km MSL and the generating cells were no longer present above the SBNY site. The MRR data indicate much lower turbulence than during the preband period and the MRR Doppler velocity profile showed a slight increase with decreasing height (Fig. 16b). Taken together, the KOKX and MRR fields indicate that the snow falling at the surface likely did not originate directly overhead but rather was advected through the column over SBNY from a neighboring area. The shift to higher values in the MRR Doppler velocity profiles from 1130 to 1200 UTC as compared to 1000 to 1130 UTC is consistent with the increasing degree of riming observed at the surface (Figs. 14e and 16b). Snow-to-liquid ratios increased to 12:1 between 1000 and 1100 UTC as the dendritic habits became more common (Fig. 14d).

3) POSTSNOWBAND (1200–1300 UTC)

As the snowband moved east of SBNY by 1200 UTC 12 January (Fig. 14a), the thermal profile cooled by ~5°C between 925 and 500 hPa (~0.75 and 5.4 km MSL; Fig. 17c) during the past few hours and the deep saturation was lost (Fig. 17a). The maximum ascent between 700 and 800 hPa (~3.0 and 2.0 km MSL; ~20 cm s^{-1}) was also weakening (Fig. 17b). Temperatures in this ascent region were between −10° to −15°C (Fig. 17c) favored more platelike crystals (~40%; Fig. 15k). Most crystals exhibited a light rime (Fig. 15l), although there were still a small amount of moderate to heavily rimed crystals toward 1300 UTC. Some of this heavier riming may be attributed to the $RH_{(ice)}$ remaining between 103% and 110% at 1200 UTC (Fig. 17b). The MRR Doppler velocity and spectral width values strengthened slightly starting at 1230 UTC. The snow-to-liquid ratio decreased from 12:1 to 8:1 by 1230 UTC with the transition from dendrites to more plates (Fig. 14d).

5. Summary and conclusions

The microphysical evolution at the surface within the comma head of two East Coast winter storms over Stony Brook, New York (SBNY), on Long Island was presented. The 19–20 December 2009 and 12 January 2011 events were associated with deepening coastal low pressure systems, and there was 48.3 and 41.3 cm of snow observed at SBNY, respectively. Surface observations of snow habit, degree of riming (0–5), and snow density were taken every 15–30 min. Within the primary snowband in the comma head forced by midlevel frontogenesis and conditional symmetric instability aloft, the changes in the maximum height of vertical motion relative to the favored ice habit growth temperatures led to rapid transitions in observed microphysics. The presnowband, snowband maturity, and postsnowband periods in both events contained many similarities. Table 1 gives a summary of the observed ice habit, degree of riming, and snow density during these periods.

During the preband periods, mostly needles were observed with a degree of riming between 1 and 3. The heavier riming occurred during the 12 January 2011 preband period, especially during the midlevel dry intrusion and shallow convective cells (0755–0930 UTC) when graupel and heavily rimed needles were observed. When the riming was light to moderate, snow-to-liquid ratios were generally from 8:1 to 9:1. The heavily rimed needles and graupel reduced the snow-to-liquid ratio to 4:1. Convective seeder ice cells developed in both events during the preband periods in a conditionally unstable environment between 400 and 600 hPa. The precipitation

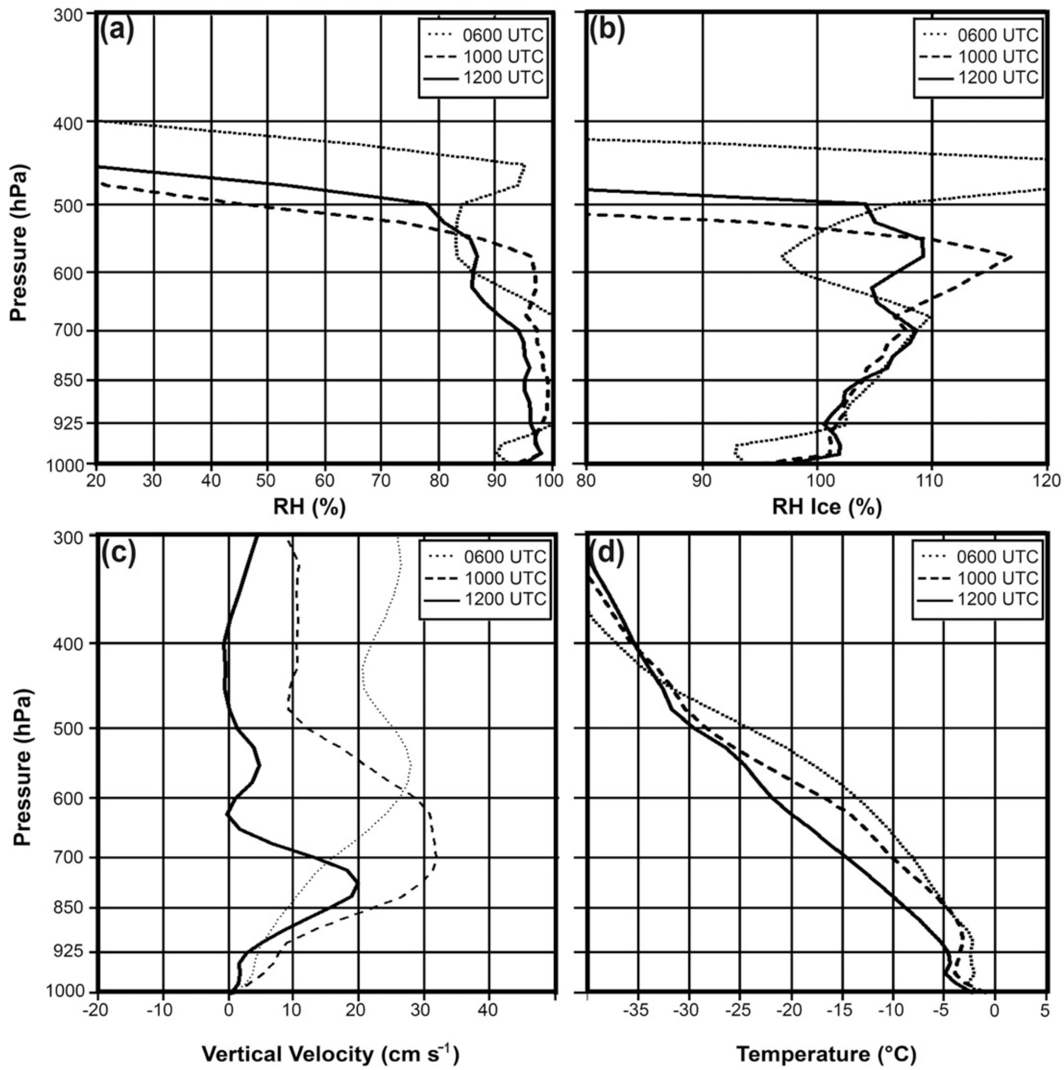

FIG. 17. As in Fig. 9, but from the 0600 UTC cycle 12 Jan 2011 12-km NAM. Dotted for 0600 UTC 12 Jan 2011, dashed for 1000 UTC 12 Jan 2011, and solid for 1200 UTC 12 Jan 2011.

rates increased as the snow from these cells descended to the surface. The snow from the cells contained a mixture of colder type crystals (bullets, columns, side planes) during the 19–20 December 2009 preband period, and more dendrites on 12 January 2011 since they formed in a slightly warmer environment than during 19–20 December.

Band maturity had a primarily dendritic snow habit. At the start of the band maturity, the degree of riming was moderate. However, as the strongest frontogenical ascent (weaker during 12 January 2011) moved east of SBNY and supersaturation began to decrease, the degree of riming decreased rapidly from moderate (i.e., 2.5–3) to light (i.e., 1). The snow-to-liquid ratios increased to between 11:1 and 13:1 during the band maturity periods.

The postsnowband periods were both characterized by a transition to a more platelike habit. The forcing for ascent, $RH_{(water)}$ and $RH_{(ice)}$ were decreasing allowing for the platelike crystals to be observed. The degree of riming was generally near 1, except a slight increase to 3 at the end of the postband period as some of the plates became moderately rimed in the 12 January 2011 event. The snow-to-liquid ratios decreased to 8:1 during the postsnowband period. In both cases, slight variations in the remaining habits were observed as described on Table 1.

Future work will investigate how well the Weather Research and Forecasting Model (WRF) BMPs can simulate the microphysical transitions during these events. Observations taken during these events will verify WRF

TABLE 1. Dominant habit, riming, and snow-to-liquid ratio for the heavy snowbands observed on 19–20 Dec 2009 and 12 Jan 2011.

Event	Preband	Maturity	Postband
19–20 Dec 2009	0000–0300 UTC Dominant habit: Needles (~40%) Riming: 1–2 Snow-to-liquid ratio: 8:1–9:1 Comments: Some bullets, side planes, and columns from seeder cells aloft	0300–0600 UTC Dominant habit: Dendrites (~55%) Riming: 1–2.5 Snow-to-liquid ratio: 11:1–13:1 Comments: Riming decreased from 2.5 to 1 between 0430 and 0445 UTC; remained ~1 through 0600 UTC	0600–0800 UTC Dominant habit: Platelike (~40%) Riming: 1 Snow-to-liquid ratio: 8:1 Comments: Some ice/miscellaneous, needles, dendrites, and side planes observed
12 Jan 2011	0600–1000 UTC Dominant habit: Needles (~50%), ~40% graupel between 0755 and 930 UTC Riming: 1–4.5 Snow-to-liquid ratio: 8:1, but 4:1 in graupel Comments: Graupel and heavily rimed needles within shallow convective cells with midlevel dry intrusion; dendrites and platelike habit with seeder cells aloft between 0600 and 630 UTC	1000–1200 UTC Dominant habit: Dendrites (~40%) Riming: 1–3 Snow-to-liquid ratio: 11:1–12:1 Comments: Riming decreased from 3 at 1000 UTC to l by 1030 UTC and remained ~1 through 1200 UTC; some needles and platelike habits observed	1200–1300 UTC Dominant Habit: Plate-like (~35%) Riming: 1–3 Snow-to-liquid ratio: 8:1 Comments: Some plates moderately rimed; some side planes, dendrites, and needles observed

simulations of riming, fall speed, snow density, and size distributions. Other work will involve a summary analysis of the microphysics during all snow events during the 2009–12 winter seasons.

Acknowledgments. Financial support for this research project was given by the National Science Foundation (ATM-0908288 for Colle and ATM-0908420 for Yuter). Special thanks to Dr. Gordon Taylor for allowing us to use his microscope and camera throughout the observational portion of this study. We thank Ashlie Sears and Nancy Furbush of NWS OKX for their help using GIS to create snowfall accumulation maps. Also, special thanks to Andrew Hall from the Cloud and Precipitation Processes and Patterns Group at North Carolina State University for his help creating the NWS radar time–heights plots.

REFERENCES

Bailey, M. P., and J. Hallett, 2009: A comprehensive habit diagram for atmospheric ice crystals: Confirmation from the laboratory, AIRS II, and other field studies. *J. Atmos. Sci.,* **66,** 2888–2899.

Baxter, M. A., C. E. Graves, and J. T. Moore, 2005: A climatology of snow-to-liquid ratio for the contiguous United States. *Wea. Forecasting,* **20,** 729–744.

Benjamin, S. G., and Coauthors, 2004: An hourly assimilation–forecast cycle: The RUC. *Mon. Wea. Rev.,* **132,** 495–518.

Cha, J., K. Chang, S. Yum, and Y. Choi, 2009: Comparison of the bright band characteristics measured by Micro Rain Radar (MRR) at a mountain and a coastal site in South Korea. *Adv. Atmos. Sci.,* **26,** 211–221.

Colle, B. A., J. B. Wolfe, W. J. Steenburgh, D. E. Kingsmill, J. A. Cox, and J. C. Shafer, 2005: High resolution simulations and microphysical validation of an orographic precipitation event over the Wasatch Mountains during IPEX IOP3. *Mon. Wea. Rev.,* **133,** 2947–2971.

Garvert, M. F., B. A. Colle, and C. F. Mass, 2005: The 13–14 December 2001 IMPROVE-2 event. Part I: Synoptic and mesoscale evolution and comparison with a mesoscale model simulation. *J. Atmos. Sci.,* **62,** 3474–3492.

Hill, F. F., K. A. Browning, and M. J. Bader, 1981: Radar and rain gauge observations of orographic rain over south Wales. *Quart. J. Roy. Meteor. Soc.,* **107,** 743–670.

Hobbs, P. V., 1975: The nature of winter clouds and precipitation in the Cascade Mountains and their modification by artificial seeding. Part I: Natural conditions. *J. Appl. Meteor.,* **14,** 783–804.

Houze, R. A., P. V. Hobbs, P. H. Herzegh, and D. B. Parsons, 1979: Size distributions of precipitation particles in frontal clouds. *J. Atmos. Sci.,* **36,** 156–162.

Judson, A., and N. Doesken, 2000: Density of freshly fallen snow in the central Rocky Mountains. *Bull. Amer. Meteor. Soc.,* **81,** 1577–1587.

Keighton, S., and Coauthors, 2009: A collaborative approach to study northwest flow snow in the southern Appalachians. *Bull. Amer. Meteor. Soc.,* **90,** 979–991.

Kneifel, S., M. S. Kulie, and R. Bennartz, 2011a: A triple-frequency approach to retrieve microphysical snowfall parameters. *J. Geophys. Res.,* **116,** D11203, doi:10.1029/2010JD015430.

——, M. Maahn, G. Peters, and C. Simmer, 2011b: Observation of snowfall with a low-power FM-CW K-band radar (Micro Rain Radar). *Meteor. Atmos. Phys.,* **113,** 75–87.

Kocin, P. J., P. N. Schumacher, R. F. Morales Jr., and L. W. Uccellini, 1995: Overview of the 12–14 March 1993 superstorm. *Bull. Amer. Meteor. Soc.,* **76,** 165–182.

Lin, Y., and B. A. Colle, 2009: The 4–5 December 2001 IMPROVE-2 event: Observed microphysics and comparisons with the Weather Research and Forecasting model. *Mon. Wea. Rev.,* **137,** 1372–1392.

Maahn, M., and P. Kollias, 2012: Improved micro rain radar snow measurements using Doppler spectra post-processing. *Atmos. Meas. Tech. Discuss.,* **5,** 4771–4808, doi:10.5194/amt-5-4771-2012.

Magono, C., and C. Lee, 1966: Meteorological classification of natural snow crystals. *J. Fac. Sci. Hokkaido Univ. Ser. 7,* **2,** 321–335.

Matrosov, S. Y., 2007: Modeling backscatter properties of snowfall at millimeter wavelengths. *J. Atmos. Sci.,* **64,** 1727–1736.

Molthan, A. L., W. A. Petersen, S. W. Nesbitt, and D. Hudak, 2010: Evaluating the snow crystal size distribution and density assumptions within a single-moment microphysics scheme. *Mon. Wea. Rev.,* **138,** 4254–4267.

Mosimann, L., E. Weingartner, and A. Waldvogel, 1994: An analysis of accreted drop sizes and mass on rimed snow crystals. *J. Atmos. Sci.,* **51,** 1548–1558.

NCDC, 2006: *Storm Data*. Vol. 48, No. 2, 134 pp.

Novak, D. R., and B. A. Colle, 2012: Diagnosing snowband predictability using a multimodel ensemble system. *Wea. Forecasting,* **27,** 565–585.

——, L. F. Bosart, D. Keyser, and J. S. Waldstreicher, 2004: An observational study of cold season–banded precipitation in northeast U.S. cyclones. *Wea. Forecasting,* **19,** 993–1010.

——, B. A. Colle, and S. E. Yuter, 2008: High-resolution observations and model simulations of the life cycle of an intense mesoscale snowband over the northeastern United States. *Mon. Wea. Rev.,* **136,** 1433–1456.

Peters, G., B. Fischer, and T. Andersson, 2002: Rain observations with a vertically looking Micro Rain Radar (MRR). *Boreal Environ. Res.,* **7,** 353–362.

——, and Coauthors, 2005: Profiles of raindrop size distributions as retrieved by Micro Rain Radars. *J. Appl. Meteor.,* **44,** 1930–1949.

Petersen, W. A., and Coauthors, 2007: NASA GPM/PMM participation in the Canadian CloudSat/CALIPSO validation project (C3VP): Physical process studies in snow. Preprints, *33rd Int. Conf. on Radar Meteorology,* Cairns, Australia, Amer. Meteor. Soc., P12A.8. [Available online at https://ams.confex.com/ams/pdfpapers/123652.pdf.]

Power, B. A., P. W. Summers, and J. d'Avignon, 1964: Snow crystal forms and riming effects as related to snowfall density and general storm conditions. *J. Atmos. Sci.,* **21,** 300–305.

Rinehart, R. E., 2004: *Radar for Meteorologists*. 4th ed. Rinehart Publications, 482 pp.

Roebber, P. J., S. L. Bruening, D. M. Schultz, and J. V. Cortinas, 2003: Improving snowfall forecasting by diagnosing snow density. *Wea. Forecasting,* **18,** 264–287.

Rutledge, S. A., and P. V. Hobbs, 1983: The mesoscale and microscale structure and organization of clouds and precipitation in midlatitude cyclones. VIII: A model for the ''seeder-feeder'' process in warm-frontal rainbands. *J. Atmos. Sci.,* **40,** 1185–1206.

Ryan, B. F. D., E. R. Wishart, and D. E. Shaw, 1976: The growth rates and densities of ice crystals between −3°C and −21°C. *J. Atmos. Sci.,* **33,** 842–850.

Schultz, D. M., and P. N. Schumacher, 1999: The use and misuse of conditional symmetric instability. *Mon. Wea. Rev.,* **127,** 2709–2732; Corrigendum, **128,** 1573.

Sienkiewicz, J. M., J. D. Locatelli, P. V. Hobbs, and B. Geerts, 1989: Organization and structure of clouds and precipitation on the mid-Atlantic coast of the United States. Part II: The mesoscale and microscale structures of some frontal rainbands. *J. Atmos. Sci.,* **46,** 1349–1364.

Stewart, R. E., and R. W. Crawford, 1995: Some characteristics of the precipitation formed within winter storms over eastern Newfoundland. *Atmos. Res.,* **36,** 17–37.

Stoelinga, M. T., and Coauthors, 2003: Improvement of microphysical parameterization through observational verification experiment. *Bull. Amer. Meteor. Soc.,* **84,** 1807–1826.

——, J. D. Locatelli, and C. P. Woods, 2007: The occurrence of ''irregular'' ice particles in stratiform clouds. *J. Atmos. Sci.,* **64,** 2740–2750.

Super, A. B., and E. W. Holroyd III, 1997: Snow accumulation algorithm for the WSR-88D radar: Second annual report. U.S. Department of Interior Bureau Reclamation Tech. Rep. R-97-05, 77 pp. [Available from National Technical Information Service, 5285 Port Royal Rd., Springfield, VA 22161.]

Takahashi, T., T. Endoh, and G. Wakahoma, 1991: Vapor diffusional growth of free-falling snow crystals. *J. Meteor. Soc. Japan,* **69,** 15–30.

Xie, X., U. Löhnert, S. Kneifel, and S. Crewell, 2012: Snow particle orientation observed by ground-based microwave radiometry. *J. Geophys. Res.,* **117,** D02206, doi:10.1029/2011JD016369.

Yuter, S. E., J. A. Crouch, B. A. Colle, and Y. Lin, 2008: Storm structure, freezing level height, and precipitation in the U.S. Pacific Northwest. *Proc. Fifth European Conf. on Radar in Meteorology and Hydrology,* Helsinki, Finland.